Check for updates

Geochemistry, Geophysics, Geosystems®

RESEARCH ARTICLE
10.1029/2025GC012881

Ediacara Obscura: Unveiling Hidden Magnetisations in the Fen Complex, Southern Norway

Justin A. D. Tonti-Filippini[1], Paul Y. J. Antonio[2], Sven Dahlgren[3,4], Rosa de Boer[5], Leandro Gallo[1], Petter Silkoset[1], Bertwin de Groot[5], Lennart de Groot[5], and Mathew Domeier[1]

[1]Centre for Planetary Habitability, University of Oslo, Oslo, Norway, [2]Géosciences Montpellier, Université de Montpellier, CNRS, Montpellier, France, [3]Njord Centre for Studies of the Physics of the Earth, University of Oslo, Oslo, Norway, [4]Telemark County Council, Skien, Norway, [5]Paleomagnetic Laboratory Fort Hoofddijk, Department of Earth Sciences, Utrecht University, Utrecht, The Netherlands

Key Points:

- The Fen complex was pervasively overprinted in the Permian (ca. 270 Ma) during tectono-magmatic activity of the Oslo Rift
- A primary, shallow paleodirection survives in several intrusions of the Fen complex not previously studied (mainly damtjernites)
- We define a new Fen pole which places Baltica near the equator ca. 583 Ma, consistent with directions from the coeval Alnö complex

Supporting Information:

Supporting Information may be found in the online version of this article.

Correspondence to:

J. A. D. Tonti-Filippini,
justinto@uio.no

Citation:

Tonti-Filippini, J. A. D., Antonio, P. Y. J., Dahlgren, S., de Boer, R., Gallo, L., Silkoset, P., et al. (2026). Ediacara obscura: Unveiling hidden magnetisations in the Fen complex, southern Norway. *Geochemistry, Geophysics, Geosystems*, *27*, e2025GC012881. https://doi.org/10.1029/2025GC012881

Received 9 JAN 2026
Accepted 6 APR 2026

Author Contributions:

Conceptualization: Justin A. D. Tonti-Filippini, Sven Dahlgren, Mathew Domeier
Data curation: Justin A. D. Tonti-Filippini, Paul Y. J. Antonio, Rosa de Boer, Leandro Gallo, Bertwin de Groot, Mathew Domeier
Formal analysis: Justin A. D. Tonti-Filippini, Paul Y. J. Antonio, Sven Dahlgren, Leandro Gallo, Mathew Domeier

© 2026 The Author(s). Geochemistry, Geophysics, Geosystems published by Wiley Periodicals LLC on behalf of American Geophysical Union.
This is an open access article under the terms of the Creative Commons Attribution-NonCommercial License, which permits use, distribution and reproduction in any medium, provided the original work is properly cited and is not used for commercial purposes.

Abstract Paleomagnetic directions found in Ediacaran (635–539 Ma) rocks are widely dispersed, which has led to conflicting hypotheses about tectonic regimes and geomagnetic field behavior during this period, and raised doubts about the fidelity of the paleomagnetic record. In particular, data from eastern and western Baltica show large and rapid changes in paleopole positions which are difficult to explain if we assume a geocentric axial dipole field operated in the Ediacaran. We present new paleomagnetic data from 214 samples across 18 sites of the Fen carbonatite-alkaline rock complex (583 ± 15 Ma) in southern Norway, coupled with detailed petrographic observations using transmitted and reflected light, scanning electron and quantum diamond microscopy, alongside conventional rock magnetic and mineralogical analyses. Our results indicate that the Fen complex and its associated intrusions were pervasively overprinted in the Permian (ca. 270 Ma), during tectono-magmatic activity of the nearby Oslo Rift, which complicated previous paleomagnetic interpretations. However, after removing secondary overprints, we find that 7% of our specimens preserve weak, shallow paleodirections interpreted as primary. The outlier directions are found in rock types not previously studied, mainly damtjernites (ultramafic lamprophyre intrusions). Based on specimen directions from these preserved units, we define a new paleopole at 266.6°E, −1.7°N (A_{95} = 4.5°, K = 77.4, N = 15), which places Baltica at low/equatorial latitudes during the mid-Ediacaran (ca. 583 Ma). Our findings have significant implications for understanding the nature of the geomagnetic field and Baltica's paleogeography in the late Neoproterozoic.

Plain Language Summary We obtained records of Earth's magnetic field preserved in 583-million-year-old rocks from southern Norway. Previous studies of similarly aged rocks from the paleocontinent of Baltica (i.e., Norway, Sweden, Ukraine and Russia) revealed scattered magnetic directions that have led to confusion about Earth's tectonic conditions and magnetic field behavior during the Ediacaran period (635–539 million years ago). We collected 214 samples across 18 sites of the Fen complex, a suite of rare igneous intrusions characterized by high carbonate content, focusing on rock types not previously studied for their magnetic properties. By employing advanced magnetic microscopy and detailed mineral analyses, alongside paleomagnetic and rock magnetic experiments, we show that most samples were affected by later tectonic and magmatic activity around 270 million years ago, which corrupted the original magnetic signature. However, 7% of the samples have retained weak, primary magnetic directions which allow us to calculate a new ancient paleomagnetic pole position for Baltica. The pole suggests that Baltica was located near the equator in the mid-Ediacaran. These findings enhance our understanding of Baltica's geological history and environmental conditions at that time.

1. Introduction

Rocks can preserve a record of Earth's ancient magnetic field, which paleomagnetists use to understand the history of the geomagnetic field, as well as reconstruct tectonic plate motions in deep time. A common assumption in paleomagnetism is that Earth's field is predominately dipolar, and that the axis of this dipole aligns with the geographic (rotational) pole when averaged over long timescales, that is, the geocentric axial dipole (GAD) hypothesis. This assumption appears to be largely valid for the past 5–10 Ma (de Oliveira et al., 2021) and potentially during much older periods, such as the Proterozoic (Evans, 2006; Gong et al., 2025; Liu et al., 2024; Meert, 2009), and even the Archean ca. 3.25 Ga (Brenner et al., 2022). The GAD assumption is useful for

15252027, 2026, 5, Downloaded from https://agupubs.onlinelibrary.wiley.com/doi/10.1029/2025GC012881, Wiley Online Library on [07/11/2026]. See the Terms and Conditions (https://onlinelibrary.wiley.com/terms-and-conditions) on Wiley Online Library for rules of use; OA articles are governed by the applicable Creative Commons License

Funding acquisition: Lennart de Groot, Mathew Domeier
Investigation: Justin A. D. Tonti-Filippini, Paul Y. J. Antonio, Sven Dahlgren, Petter Silkoset
Methodology: Justin A. D. Tonti-Filippini, Paul Y. J. Antonio, Sven Dahlgren, Rosa de Boer, Leandro Gallo, Petter Silkoset, Bertwin de Groot, Mathew Domeier
Project administration: Justin A. D. Tonti-Filippini, Lennart de Groot, Mathew Domeier
Resources: Paul Y. J. Antonio, Sven Dahlgren, Lennart de Groot, Mathew Domeier
Software: Justin A. D. Tonti-Filippini, Paul Y. J. Antonio, Leandro Gallo, Bertwin de Groot, Mathew Domeier
Supervision: Sven Dahlgren, Lennart de Groot, Mathew Domeier
Visualization: Justin A. D. Tonti-Filippini, Paul Y. J. Antonio, Rosa de Boer, Leandro Gallo, Bertwin de Groot, Mathew Domeier
Writing – original draft: Justin A. D. Tonti-Filippini
Writing – review & editing: Justin A. D. Tonti-Filippini, Paul Y. J. Antonio, Sven Dahlgren, Rosa de Boer, Leandro Gallo, Lennart de Groot, Mathew Domeier

reconstructing Earth's paleogeography, for example, tracking past positions and movements of tectonic plates; the formation and breakup of supercontinents; and monitoring rotation of the entire solid Earth, that is, true polar wander (TPW).

However, there are periods of time where the paleomagnetic record appears to behave erratically, which poses a challenge to several fundamental assertions, namely that: (a) Earth's magnetic field can be approximated by a GAD field (Creer et al., 1957; Hospers, 1954; Runcorn, 1962); (b) individual plate motions are limited to <20 cm/yr (Torsvik et al., 2012; Zahirovic et al., 2015); (c) maximum TPW rates are typically of order 2.5°/Myr (Phillips et al., 2009; Tsai & Stevenson, 2007); and (d) the paleomagnetic record can generally be relied upon, assuming there are sufficient sampling opportunities in relatively undeformed and unmetamorphosed rocks from the desired time period (Meert et al., 2020; Van Der Voo, 1990). One of the most complicated periods is the Ediacaran (635–539 Ma), where published paleomagnetic directions are widely dispersed and sometimes orthogonal to each other, even from rocks of similar ages found on the same continent and, in some cases, rocks from the same formation (e.g., Halls et al., 2015; Robert et al., 2023). Significant upheavals in Earth's environmental conditions are also observed during this period, which some have suggestively linked to extraordinary behavior of the geomagnetic field (e.g., Tarduno et al., 2025).

Recent studies suggest that the Ediacaran field was extremely weak (Huang et al., 2024; Thallner et al., 2021) and perhaps intermittently non-dipolar (Abrajevitch & Van der Voo, 2010; Robert et al., 2023). Ediacaran paleodirections from Baltica exemplify this strange behavior (Figure 1a) and are difficult to explain in the context of the assertions listed above (Domeier et al., 2023). In particular, directions from western Baltica, that is, Norway and Sweden (Meert et al., 1998, 2007), are inconsistent with each other and at odds with directions from eastern Baltica, mainly Russia and Ukraine (Fedorova et al., 2014; Iosifidi et al., 2005; Levashova et al., 2013, 2015; Llanos et al., 2005; Lubnina et al., 2014; Popov et al., 2002, 2005). Resolving these directions is important for understanding the long-term behavior of the geomagnetic field, and Earth's history in general. For example, Baltica hosts the Mortesnes and Moelv tillites, which have been correlated with Ediacaran glaciations (Agić et al., 2024; Bingen et al., 2005), so determining Baltica's paleolatitude during this time has implications for determining the extent of Ediacaran glaciations and whether they could have progressed to the magnitude of a snowball Earth event (Kirschvink, 1992; Meert & Torsvik, 2004; Pu et al., 2016).

Two key sites in western Baltica are the carbonatite complexes of Fen and Alnö (Figure 1b), where previous paleomagnetic studies yielded conflicting results (Meert et al., 1998, 2007; Piper, 1981, 1988; Poorter, 1972). Both complexes intruded basement rocks in the western interior of the Baltica craton and have been dated to similar ages (ca. 583–584 Ma), so one would expect them to contain similar paleomagnetic records. However, the complexes contain three orthogonal clusters of paleodirections (Figure 1a). The Fen complex contains mid-inclination SSW-up directions, based on sampling of phonolites/tinguaites (Meert et al., 1998; Piper, 1988) and the rødberg ("red rock") formation (Poorter, 1972). Meanwhile, Alnö contains scattered paleodirections which vary from steep/vertical down to shallow/horizontal WNW and ESE (Meert et al., 2007; Piper, 1981). The data of Piper (1981) suggests that the Alnö directions vary with rock type, with most of the shallow directions found in alnöites (lamprophyres) and søvites (calcite-carbonatites). Meert et al. (2007) did not differentiate Alnö directions by rock type, but grouped the directions into steep and shallow subsets, without concluding if either subset was primary or secondary.

Importantly, recent compilations of Ediacaran paleomagnetic data (e.g., Domeier et al., 2023; Levashova et al., 2013; Meert, 2014) exclude paleopoles from Fen and Alnö due to their contradictory nature, yet being able to confidently incorporate these poles is crucial, as their omission leaves a significant gap in the Ediacaran paleomagnetic record of Baltica. Directions from the Fen complex are well-clustered but suspiciously similar to those obtained from nearby Permo-Carboniferous rocks of the Oslo Rift (Torsvik et al., 1998). The Alnö directions are not well-clustered, but the steep directions overlap with the present-day field direction (Meert et al., 2007). The shallow Alnö directions possess dual-polarities and define a pole unique to any younger poles or known overprints, suggesting they may be primary, but are quite different to directions obtained from the Egersund dikes in western Norway, baddeleyite U-Pb dated to 616 ± 3 Ma (Walderhaug et al., 2007), and other Ediacaran rocks from eastern Baltica (Levashova et al., 2013). None of the previous Fen or Alnö studies included field tests to assess the primary character of the magnetisations (i.e., fold, reversal or conglomerate tests).

To shed light on the obscure and contradictory paleomagnetic record of the Fen complex, we present new data from 18 sites (Figures 1c and 1d), focusing on carbonatite and fresh alkaline silicate rocks at localities not sampled

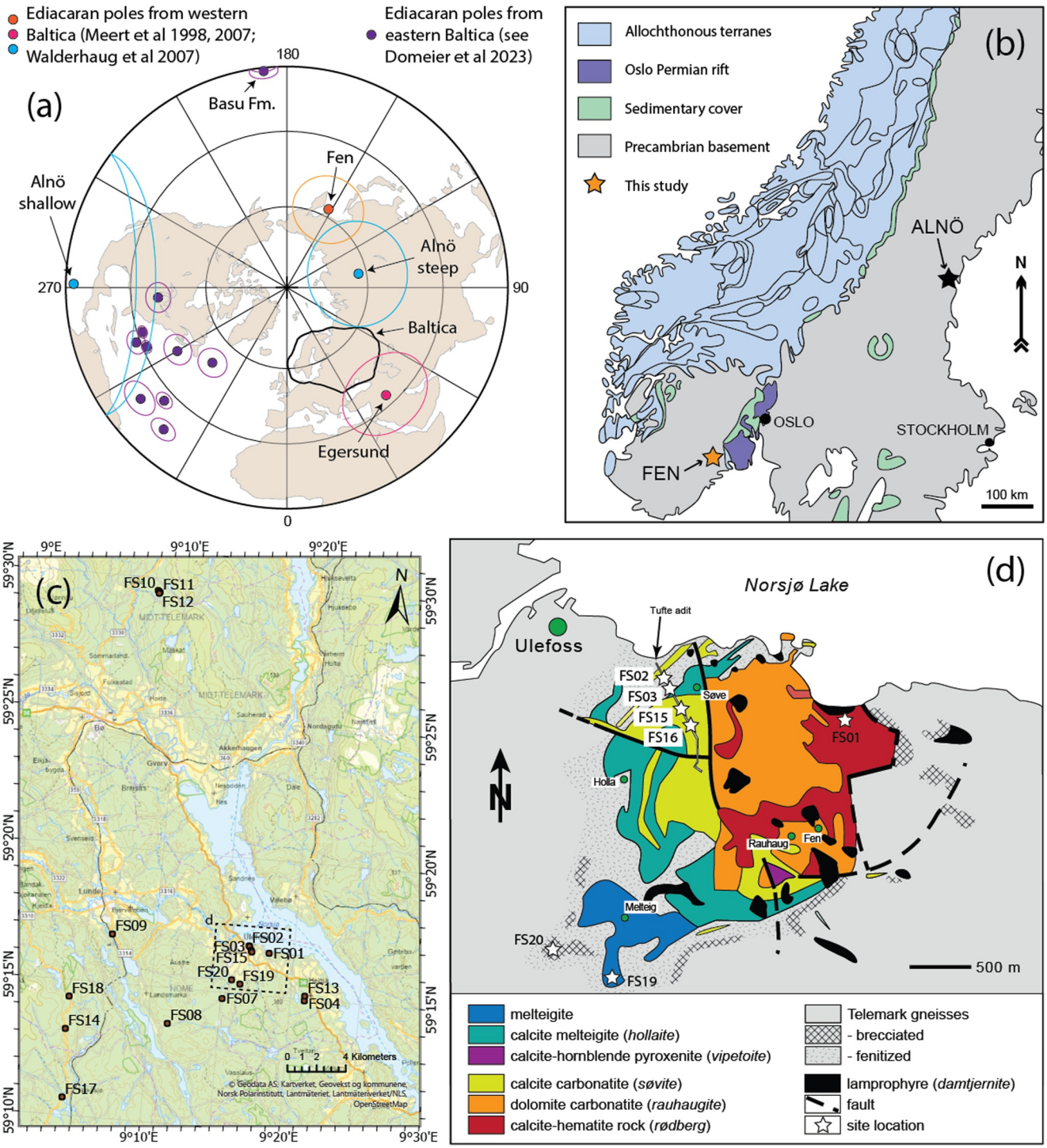


Figure 1. (a) Ediacaran poles from previous studies on western Baltica (Meert et al., 1998, 2007; Walderhaug et al., 2007) and eastern Baltica (Domeier et al., 2023, and references therein). Poles from the Fen and Alnö carbonatite complexes are distinctly different from each other, and at odds with poles from eastern Baltica. (b) Overview map of the Fen (southern Norway) and Alnö (central Sweden) carbonatite complexes (after Gee et al., 2010). Both locations are >200 km from the Caledonian thrust front. (c) Overview map of sampling sites in this study. (d) Map of the Fen main complex with sampling sites from this study (after Sæther, 1957; Barth & Ramberg, 1966) (modified from Dietzel et al., 2019).

15252027, 2026, 5, Downloaded from https://agupubs.onlinelibrary.wiley.com/doi/10.1029/2025GC012881, Wiley Online Library on [07/11/2026]. See the Terms and Conditions (https://onlinelibrary.wiley.com/terms-and-conditions) on Wiley Online Library for rules of use; OA articles are governed by the applicable Creative Commons License

15252027, 2026, 5, Downloaded from https://agupubs.onlinelibrary.wiley.com/doi/10.1029/2025GC012881, Wiley Online Library on [07/11/2026]. See the Terms and Conditions (https://onlinelibrary.wiley.com/terms-and-conditions) on Wiley Online Library for rules of use; OA articles are governed by the applicable Creative Commons License

by previous studies, as well as resampling of three sites studied by Meert et al. (1998). For comparison, we also sampled two younger diabase dikes intruding the complex, presumably Permo-Carboniferous (ca. 310-240 Ma) in age (Sundvoll & Larsen, 1990, 1994); perovskite U-Pb dating of a tuff at the base of the nearby Skien lavas (10 km away) yielded an age of 298.9 ± 0.7 Ma (Corfu & Dahlgren, 2008). Seven of our sites included baked contact tests (three within 4 km of the main complex, and four 10–25 km away). The samples were subjected to detailed paleomagnetic, rock magnetic, and mineralogical analyses, including micromagnetic observations using a quantum diamond microscope (QDM). We aimed to: (a) determine if different paleomagnetic directions could be found in Fen rock types not previously sampled; and (b) characterize the nature of the SSW-up directions previously reported and assess if they are primary or secondary. We compare our findings with the previous studies of Fen and Alnö, and discuss their implications with respect to the nature of the geomagnetic field and the paleogeography of Baltica in the Ediacaran.

2. Geological Context

2.1. The Fen Complex

The Fen complex is a carbonatite - alkaline silicate rock complex located 150 km southwest of Oslo, Norway, first described by Brøgger (1921). The main complex is roughly circular with a diameter of ca. 4 km (Figure 1d), where different carbonatites and alkaline silicate rocks were emplaced into Mesoproterozoic basement rocks and pervasively alkali-metasomatized the surrounding area, a process known as fenitisation now recognised in host rocks adjacent to carbonatites worldwide. The Fen complex hosts global type localities for fenite, as well as søvite (calcite-phlogopite carbonatite), damtjernite (ultramafic lamprophyre), rauhaugite (dolomite carbonatite), and melteigite (foidolite), named after nearby farms (Brøgger, 1921). The various rocks of the main complex have been hydrothermally altered to a variable degree during at least two events (Dietzel et al., 2019).

Ongoing remapping of the Fen main complex has revealed that it developed in five major phases (Dahlgren, 2019):

1. Intrusion of alkaline silicate rocks and associated pyroxene-calcite carbonatites
2. Intrusion of søvite and rauhaugite carbonatite dikes
3. Emplacement of Fe-dolomite carbonatites (FDC), which are extensively REE-mineralized
4. Intrusion of damtjernites
5. Hydrothermal alteration and hematite ore formation, also generating the hematized “red rocks”

The Fen complex was most recently dated to 583 ± 15 Ma (Meert et al., 1998), a combined interpretation based on Ar-Ar dating of phlogopite (589.1 ± 0.5 Ma) and biotite (578.3 ± 0.8 Ma), which is similar to the age of Alnö, 584 ± 7 Ma, based on Ar-Ar dating of biotite (Meert et al., 2007). It is assumed that these mica Ar-Ar ages closely approximate the timing of emplacement, and that neither complex has experienced high temperatures since emplacement, given biotite has closure temperatures between 280 and 345°C for Ar (Harrison et al., 1985). $\delta^{18}O$ data from the rauhaugites and søvites in the Fen complex indicate temperatures for the magmatic stage of 600–700°C, while data for rødberg indicate hydrothermal formation around 200–300°C (Fredrichsen, 1968). Both Fen and Alnö stand >200 km away from the Caledonian thrust front (Figure 1b), which magnetically overprinted much of Scandinavia to the west (Bylund & Zellman, 1980; de Wall & Greiling, 2000). However, the Fen complex lies on the SW edge of the Permo-Carboniferous Oslo Rift zone (Figure 1b), and undated diabase dikes assumed to be related to the rifting event are found in the main complex and surrounding areas. The Oslo Rift is a Late Carboniferous to Permian (ca. 310–240 Ma) extensional tectonic structure in southeastern Norway, covering approximately 3,000 km^2, and formed during post-Caledonian lithospheric thinning with extensive volcanic and sedimentary infill (Neumann et al., 1992).

A large number of satellite intrusions occur in the basement surrounding the Fen main complex, up to ca. 50 km away (Dahlgren, 1987, 1994). All these satellites are situated within the heavily fractured/faulted basement southwest of the plutons of the Oslo Rift, and most of the intrusions have also been affected by hydrothermal alteration which most likely occurred during the Late Paleozoic (Dahlgren, 1987). For simplicity we refer to the sheet intrusions as dikes, although their dip angles range from sub-vertical to sub-horizontal, with no obvious pattern to their orientation.

15252027, 2026, 5, Downloaded from https://agupubs.onlinelibrary.wiley.com/doi/10.1029/2025GC012881, Wiley Online Library on [07/11/2026]. See the Terms and Conditions (https://onlinelibrary.wiley.com/terms-and-conditions) on Wiley Online Library for rules of use; OA articles are governed by the applicable Creative Commons License

3. Methodology

3.1. Sampling Strategy

The sites for this study were selected on the basis of ongoing field mapping combined with extensive petrographic and geochemical investigations. In the Fen main complex most rocks are unexposed, and the few exposures that occur are variably weathered saprolites where the rocks are not fully in situ. Consequently, sampling was mostly performed in fresh road-cuts or within the Tufte adit which was excavated during underground niobium mining in the 1950s. Sampling of the satellite dikes focused on domains within the intrusions which displayed the least hydrothermal alteration, as recognised during previous studies of thin sections across several hundred sites. One exception is the Lunnebruene phonolite dike (FS07) which is severely hydrothermally altered, but it was not known if the alteration was post-magmatic or from some later event.

3.2. Paleomagnetism

214 paleomagnetic cores were drilled with portable gasoline and electric drills across 18 sites of the Fen complex during multiple field campaigns between 2023 and 2025. All cores were oriented with sun (when possible) and magnetic compasses. The median declination offset between the two orientation methods is +4.25° ($\sigma = 7.99°$), similar to the expected local offset of +4.2° according to the International Geomagnetic Reference Field (Alken et al., 2021), and declinations were corrected accordingly. Large deviations of up to 20° were observed in the strongly magnetic damtjernites. Four sites were located underground in the Tufte adit (FS02, FS03, FS15, FS16) where only magnetic readings could be obtained.

Cores were cut into 2.2 cm high specimens with a non-magnetic saw and prepared for analysis at the Ivar Giæver Geomagnetic Laboratory (IGGL) at the University of Oslo (Norway). Alternating field (AF) demagnetization was performed on a 2G Enterprises superconducting magnetometer or an AGICO LDA5 and JR-6A spinner magnetometer. Thermal demagnetization (TH) was performed using a magnetically shielded MMTD80 paleomagnetic oven, with subsequent measurements made on the 2G or JR-6A depending on remanence strength. Room temperature susceptibilities after each heating step were measured with a Bartington MS2 susceptibility meter. All measurements were carried out inside magnetically shielded cages with total residual fields <700 nT. Data visualization and analyses were performed with Paleomac (Cogné, 2003), Remasoft (Chadima, 2006), PmagPy (Tauxe et al., 2016) and custom Python scripts.

In line with previous studies of the Fen complex, we report all directions in geographic (in situ) coordinates and do not apply any structural tilt corrections. The Fen intrusions cut Mesoproterozoic basement with no preserved stratigraphy or primary layering that could be used to define a reliable tilt correction, and regional geological mapping around Fen does not document any systematic tilting or folding of the basement. Although it cannot be ruled out, we expect that any undetected tilting is likely to be small, and that the potential effect on our derived directions would be within or comparable to the stated uncertainties.

3.3. Rock Magnetism

Based on the paleomagnetic results, 20 specimens were selected for rock magnetic characterization to represent a range of different rock types and magnetic carriers. Unsieved powders and chips were analyzed on a Princeton Measurements Vibrating Sample Magnetometer (VSM) to obtain hysteresis loops and backfield remanence curves with fields up to 1.5 T. Unmixing of backfield curves was carried out with MAX UnMix (Maxbauer et al., 2016). Thermal susceptibility curves up to 700°C were measured with an AGICO MFK1, either in air or argon gas. Low temperature and First-Order-Reversal-Curve (FORC) measurements were performed on nine specimens using a sensitive Quantum Design Magnetic Properties Measurement System (MPMS3) at the University of Montpellier (France). A 2.5 T DC field was used to perform the following acquisition curves: field cooled (FC), zero field cooled (ZFC), and room temperature saturation isothermal remanent magnetisation during cooling (RTSIRMcool) and warming (RTSIRMwarm).

3.4. Electron and Magnetic Imaging

Petrographic observations were made on 13 thin sections, with nominal thicknesses of 30–50 μm, using a Hitachi SU5000 field-emission scanning electron microscope (FE-SEM) equipped with a dual Bruker Quantax XFlash 30 EDS system at the University of Oslo. Energy-dispersive X-ray spectroscopy (EDS) mapping was used to

15252027, 2026, 5, Downloaded from https://agupubs.onlinelibrary.wiley.com/doi/10.1029/2025GC012881, Wiley Online Library on [07/11/2026]. See the Terms and Conditions (https://onlinelibrary.wiley.com/terms-and-conditions) on Wiley Online Library for rules of use; OA articles are governed by the applicable Creative Commons License

investigate mineralogical compositions at the microscale, enabling identification and detailed characterization of mineral phases and their spatial distribution.

Micromagnetic maps were obtained using a quantum diamond microscope (QDM) at Fort Hoofddijk, Utrecht University (Netherlands), with a set-up similar to Glenn et al. (2017). The QDM is located in a shielded room, with a maximum residual field of 400 nT, and has a spatial resolution of 1.2 μm. To remove surface contamination, samples were heated to 100°C prior to analyses. After scanning samples in an NRM (natural remanent magnetisation) state, various IRM pulses up to 100 mT along the plane of the thin sections were applied using a PM4 Pulse Magnetizer and then rescanned to characterize magnetisation sources. Bias fields of 0.9 or 1.6 mT were applied depending on sample remanence strength, with the polarity of the applied field switching during measurements to remove induced magnetisation. The obtained magnetic image is converted to a map with the vertical component of the magnetic flux for interpretation.

4. Results and Observations

4.1. Petrography and Mineralogy

A summary of the petrography for key sampled units is presented in Supporting Information S1 Section A, with the petrographic details of a selection of cores used in this study in Tables S1-S3 in Supporting Information S1.

4.2. Paleomagnetic Results

236 specimens were demagnetized and analyzed with principal component analysis (PCA) (Kirschvink, 1980) and the combined analysis of great circles and direct observations (McFadden & McElhinny, 1988), summarized in Table 1 and Figures 2–4. Best fit lines were not anchored to the origin, except in three cases where the directions did not unblock toward the origin (discussed below). Paleomagnetic directions determined by PCA were similar across all sites in the Fen complex, regardless of age or rock type, with most specimens containing two distinct components (A and B). However, after unblocking components A and B, four sites appear to contain weak relict magnetisations, which cluster in a shallow westerly paleodirection, referred to as component C. Additionally, two of the contact tests revealed another unique and stable paleodirection in the host rocks which we refer to as component D.

4.2.1. Component A (Steep Northerly Down)

Component A is found in 95% of the specimens and presents steep northerly down directions (in geographic coordinates) which overlap with the expected present-day field direction (Figure 4a, Table S5 in Supporting Information S1). The component unblocks below 15 mT (with AF) or 300–400°C (with TH), consistent with viscous remanence behavior. However, in some samples the component persists up to higher fields (e.g., up to 45 mT in sample FS04K2) or temperatures (e.g., up to 550°C in FS11J1), usually unblocking along a great circle path toward the direction of component B.

4.2.2. Component B (Mid-Inclination SSW Up)

Component B is found in 85% of the specimens and presents mid-inclination south to south-west (SSW) up directions in geographic coordinates. The component generally unblocks below 60 mT (with AF) or up to 580°C (with TH), consistent with the unblocking ranges of magnetite. However, component B often unblocks at temperatures as low as 550°C (particularly in the damtjernites, FS04 and FS13), suggesting that Ti-poor titanomagnetite is also a significant remanence carrier. Occasionally, the component does not fully unblock with AF, with 20%–60% of the remanence remaining at 150 mT (Figures 2e and 23c); in these cases ($n = 19$), subsequent thermal demagnetization unblocks the remaining component between 300 and 350°C, consistent with the unblocking temperature of pyrrhotite. In four other specimens (FS14J1, FS14M1, FS16C2 and FS18A1), component B is stable until 680°C, consistent with the unblocking temperature of hematite.

In Figure 4c specimen directions for component B are grouped by remanence carrier, based on their thermal unblocking behavior ($n_{\text{magnetite}} = 139$, $n_{\text{hematite}} = 4$, $n_{\text{pyrrhotite}} = 19$). Using the method of Tauxe (2010), we tested for common true mean directions (CMTD) for the three groups with 1,000 bootstrapped Cartesian coordinates (Figures S1–S2 in Supporting Information S1). The magnetite and hematite collections overlap with 95%

Table 1
Summary of Paleomagnetic Results for ChRMs in the Fen Complex

Site	Name (MS)	Type	D_g	I_g	α_{95}	n (n_L/n_P)	CT
Component B (intrusions only)							
FS01[a]	Fenbukta	diabase	195.8	−65.9	5.9	4 (4/0)	Neg.
FS02	Tufte adit 1	mafic foidite	212.2	−40.2	11.0	7 (7/0)	
FS03	*Tufte adit 2*	*søvite*	*190.5*	*−58.3*	*32.2*	*2 (2/0)*	
FS04	Helgja 1	damtjernite	196.1	−25.0	3.7	33 (22/11)	Neg.
FS07	Lunnebruene	phonolite	202.0	−52.8	13.6	8 (6/2)	
FS08	Siljekleiv (PS2)	phonolite	196.2	−46.8	5.6	11 (11/0)	
FS09	Tyri (PS6)	phonolite	205.7	−48.9	4.0	9 (9/0)	
FS10	Kåsa (DS27)	damtjernite	196.8	−36.2	8.6	9 (4/5)	
FS11	Brånan 1	damtjernite	210.9	−37.2	7.6	11 (6/5)	Inc.
FS12	Brånan 2	damtjernite	203.9	−30.5	5.4	9 (9/0)	Inc.
FS13	Helgja 2	damtjernite	194.2	−25.5	6.2	9 (7/2)	Inc.
FS14	Drangedal 1	phonolite	205.7	−22.7	4.9	12 (5/7)	Inc.
FS15	Tufte adit 3	søvite/FDC	202.4	−57.0	7.4	10 (8/2)	
FS16	Tufte adit 4	FDC	200.9	−42.6	7.5	6 (6/0)	
FS17	Drangedal 2	phonolite	197.4	−39.3	13.4	8 (5/3)	
FS18[a]	Drangedal 3	diabase	207.3	−55.2	5.7	5 (5/0)	Inc.
FS19	Melteig	melteigite	195.4	−35.4	6.9	10 (10/0)	
FS20	Briskemyr 3	fenite	196.1	−49.2	7.6	4 (4/0)	
Component C (intrusions and contact zones)							
FS04	Helgja 1	damtjernite/gneiss	286.4	−16.8	3.4	7 (1/6)	
FS13	Helgja 2	damtjernite/gneiss	291.2	−9.9	17.9	3 (1/2)	
FS14	Drangedal 1	phonolite	267.7	−10.0	22.3	3 (1/2)	
FS15	*Tufte adit 3*	*FDC*	*268.8*	*−26.2*	*13.2*	*2 (1/1)*	
Component D (host rocks)							
FS11[b]	Brånan 1	quartzite	255.4	−40.5	10.5	3 (3/0)	
FS14[b]	Drangedal 1	gneiss	293.9	−59.8	12.5	4 (4/0)	
Component means							
	Comp. A	site mean	351.7	77.0	7.1	15 sites	
	Comp. B	site mean	201.1	−41.9	5.7	17 sites	
	Comp. C	*site mean*	*281.5*	*−12.2*	*19.3*	*3 sites*	
	Comp. C	specimen mean	278.4	−16.2	6.2	15 (4/11)	

Note. MS = site name published by Meert et al. (1998). D_g/I_g and α_{95} = declination/inclination (°) in geographic (in situ) coordinates and 95% uncertainty of Fisher (1953) mean. n_L/n_P = number of lines/planes determined with principal component analysis (PCA). CT = contact test result according to baked contact profile test definition of Buchan (2007), where neg. = negative and inc. = inconclusive. Results in italics are not considered statistically robust (n is too low) and are not used to calculate site mean directions. Results from FS15 are included in the specimen mean for comp. C. Site coordinates are listed in Table S4 in Supporting Information S1. FDC = Fe-dolomite carbonatite. [a]Younger diabase intrusion (not Fen-aged). [b]Older host (basement) rocks.

15252027, 2026, 5, Downloaded from https://agupubs.onlinelibrary.wiley.com/doi/10.1029/2025GC012881, Wiley Online Library on [07/11/2026]. See the Terms and Conditions (https://onlinelibrary.wiley.com/terms-and-conditions) on Wiley Online Library for rules of use; OA articles are governed by the applicable Creative Commons License

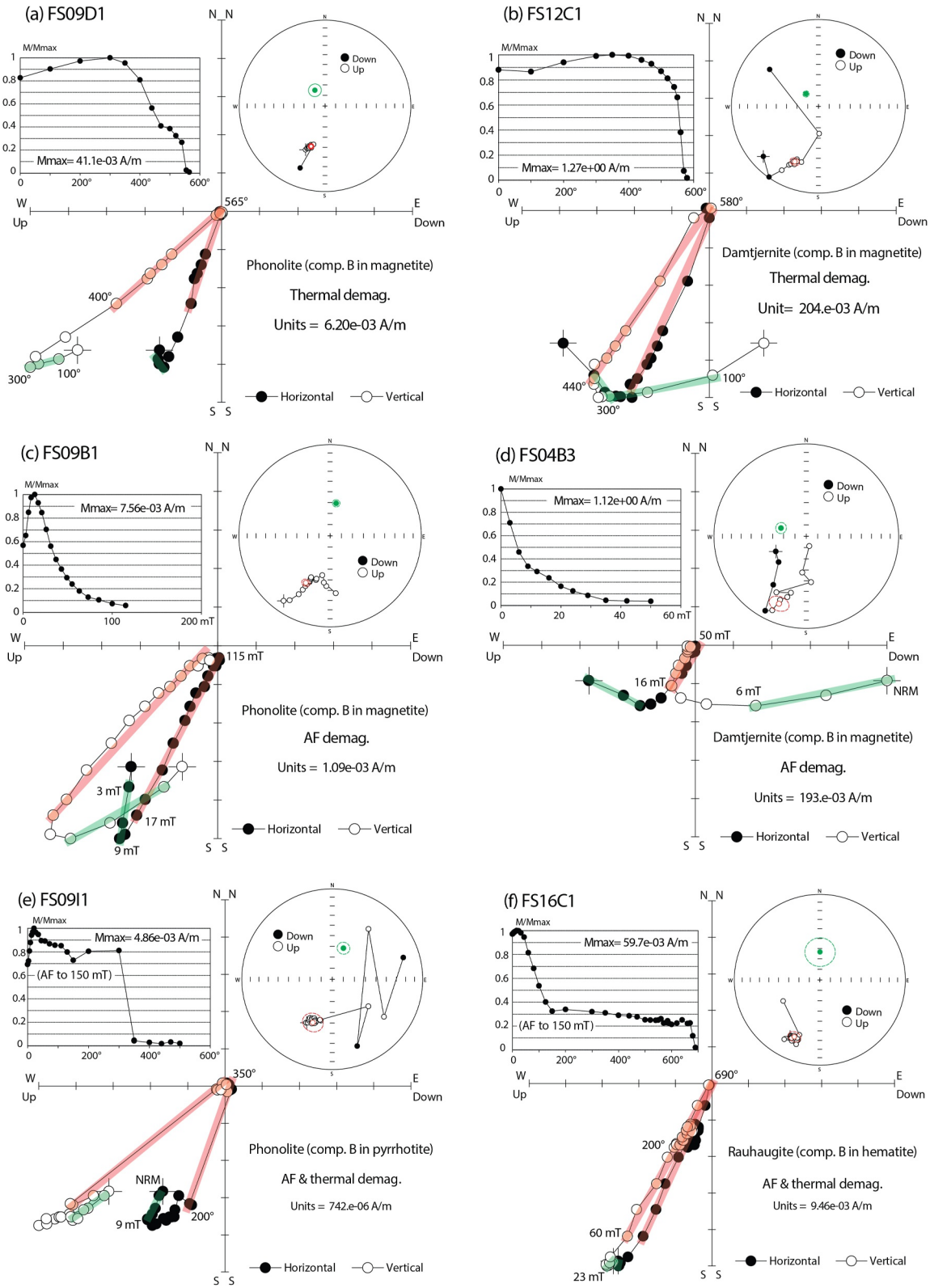


Figure 2.

15252027, 2026, 5, Downloaded from https://agupubs.onlinelibrary.wiley.com/doi/10.1029/2025GC012881, Wiley Online Library on [07/11/2026]. See the Terms and Conditions (https://onlinelibrary.wiley.com/terms-and-conditions) on Wiley Online Library for rules of use; OA articles are governed by the applicable Creative Commons License

15252027, 2026, 5, Downloaded from https://agupubs.onlinelibrary.wiley.com/doi/10.1029/2025GC012881, Wiley Online Library on [07/11/2026]. See the Terms and Conditions (https://onlinelibrary.wiley.com/terms-and-conditions) on Wiley Online Library for rules of use; OA articles are governed by the applicable Creative Commons License

confidence, while the pyrrhotite collection overlaps with neither. However, the three collections overlap with the site mean directions for component B (Table 1), suggesting they are all contemporaneous.

4.2.3. Component C (Shallow Westerly up)

Component C is present in 15 (7%) of the specimens and is faint, appearing at less than 5%–10% of the total NRM, after unblocking components A and B. Component C is only observed during TH and never with AF alone. Due to the low number of sites carrying component C, the mean direction in Table 1 was calculated using the combined analysis of 11 great circles and 4 direct observations (McFadden & McElhinny, 1988). These directions are revealed in two damtjernites (FS04, FS13), a FDC (FS15) and a distal phonolite (FS14). The great circle behavior occurs after component B unblocks below 520–560°C, above which remanence directions move progressively along subparallel great circles toward a shallow westerly direction, before the directions become unstable (randomised) above 590°C (Figures 3a–3d). However, in two specimens, the great circle behavior occurs at lower temperatures (between 400 and 540°C) after AF.

The direct observations (linear fits) are found very rarely. Only in one specimen (FS13C1) does component C unblock fully to the origin, up to 575°C (after AF to 85 mT), from the contact of a damtjernite (Figure 3e). In three other specimens (FS04N1, FS14C2 and FS15G1) the direction stabilizes but only partially unblocks toward the origin before becoming unstable above 560–575°C; in these cases the component was artificially forced to the origin. FS14C2 is from a phonolite, while FS15G1 is from a FDC—in both specimens component C stabilized between 540 and 575°C. FS04N1 is from the slightly thermally affected contact of a gneiss intruded by a damtjernite, where component C stabilized between 440 and 560°C, after AF to 150 mT (Figure 3c). These four linear fits were used to anchor the end points of the great circles to define the combined mean (Figure 4d).

Due to the low number of successful determinations (linear fits), the uncertainty in the component C pole is calculated using an adaptation of the combined (lines and planes) analysis method of McFadden and McElhinny (1988); we apply the method in pole space rather than directional space (by transforming the great circles into "VGP rings"). However, as recognised by McFadden and McElhinny (1988), the resulting precision parameter K and uncertainty circle A95 may underestimate the true uncertainty of the pole. We therefore regard the reported statistics as optimistic, so the uncertainty around the component C pole should be interpreted with caution, but still consider the combined solution to be the best estimate of the mean pole, as it uses all available information in a standard and widely accepted framework.

4.2.4. Component D (Mid-inclination Westerly up)

Component D is not found within the intrusions but is present in some of the host rocks sampled for baked contact tests (Section D in Supporting Information S1). In three specimens from a quartzite hosting a damtjernite intrusion (FS11), stable mid-inclination westerly and up directions (in geographic coordinates) fully demagnetized to the origin from 0 to 690°C, consistent with hematite, with small (20%–30%) decreases in remanence at 550°C, consistent with Ti-poor titanomagnetite, and 590°C, consistent with pure magnetite (Figure 3f). Four similar, but slightly steeper directions were found in a gneiss hosting a damtjernite intrusion (FS14), unblocking up to 560°C, consistent with titanomagnetite. Components A-C were not observed in samples carrying component D.

4.2.5. Contact Tests

We carried out baked contact tests at seven sites, including five Fen-aged intrusions and two younger diabase dikes. All seven tests were negative or inconclusive for component B (Section D in Supporting Information S1). At two sites inside or close to (within <4 km of) the Fen main complex (FS01, FS04), component B was found within the intrusions and in the host rocks up to 20 m away (more than 10 dike widths), yielding negative contact tests. The other five tests were inconclusive (although component B was found in the wall rocks immediately

Figure 2. Representative Zijderveld (1967) diagrams for specimens containing components A (green) and B (red), with remanence and stereonet plots inset. Fitted directions are shown with their MAD circles (dashed lines). (a, b) FS09D1 and FS12C1 unblock component A below 300°C and component B between 550 and 580°C (TH only). (c, d) FS09B1 and FS04B3 unblock component A below 10 mT and component B between 17–115 mT and 16–50 mT (AF only), respectively. (e) FS09I1 unblocks component B between 300 and 350°C, after AF up to 150 mT, indicating pyrrhotite as a remanence carrier. (f) FS16C1 unblocks component B up to 690°C, after AF to 150 mT, indicating hematite as a remanence carrier.

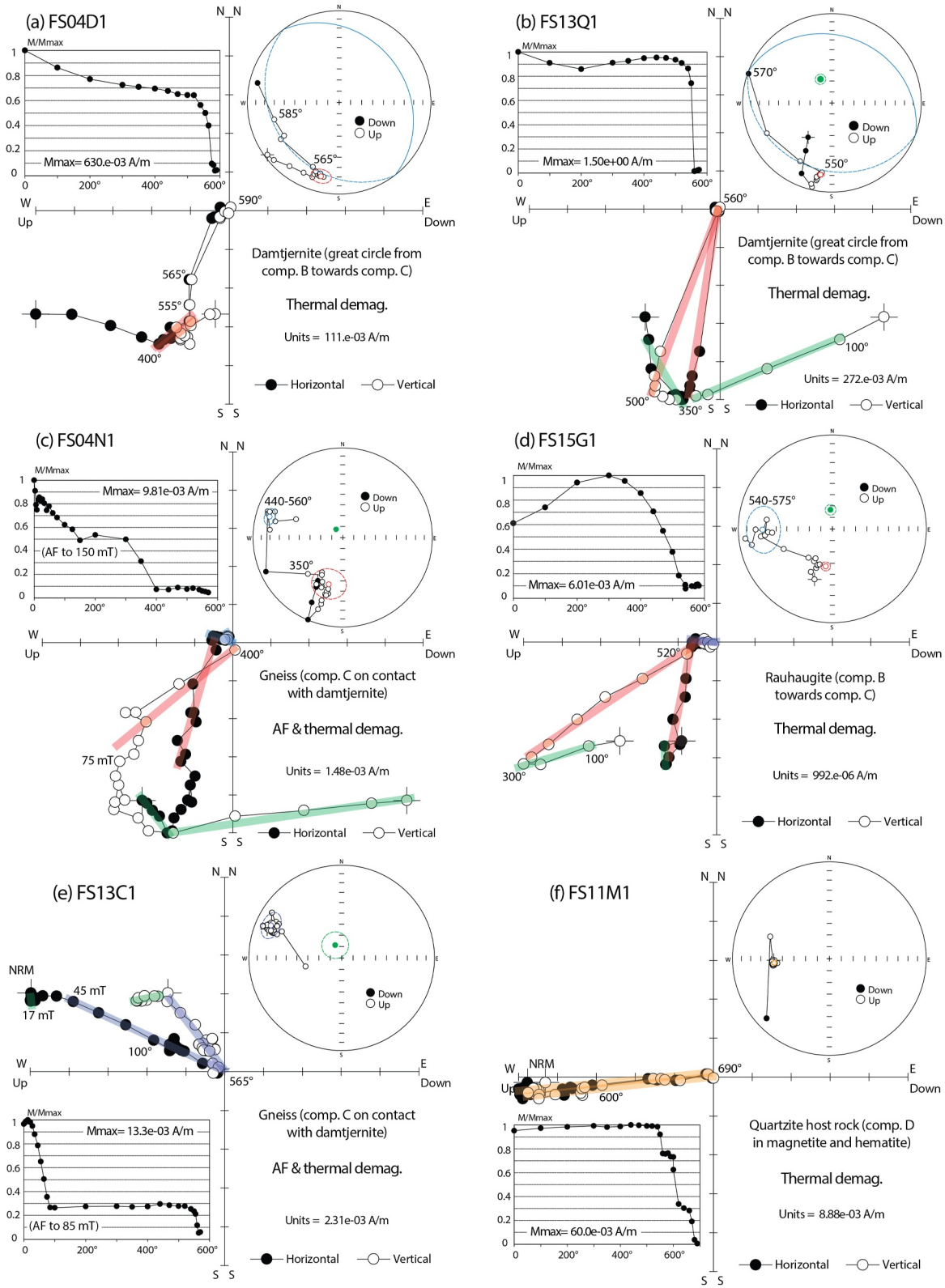


Figure 3.

15252027, 2026, 5, Downloaded from https://agupubs.onlinelibrary.wiley.com/doi/10.1029/2025GC012881, Wiley Online Library on [07/11/2026]. See the Terms and Conditions (https://onlinelibrary.wiley.com/terms-and-conditions) on Wiley Online Library for rules of use; OA articles are governed by the applicable Creative Commons License

15252027, 2026, 5, Downloaded from https://agupubs.onlinelibrary.wiley.com/doi/10.1029/2025GC012881, Wiley Online Library on [07/11/2026]. See the Terms and Conditions (https://onlinelibrary.wiley.com/terms-and-conditions) on Wiley Online Library for rules of use; OA articles are governed by the applicable Creative Commons License

adjacent to the FS12, FS13, FS14, and FS18 intrusions) as they did not meet the requirements for definitive baked contact profile tests (Buchan, 2007). Component C was found in three of the damtjernite contact samples (from FS04 and FS13), less than 50 cm away from the intrusion, but only observed with thermal demagnetization after AF treatment.

4.3. Rock Magnetic Results

Detailed rock magnetic measurements were made on 20 selected samples spanning most of the major rock types, including diabase (FS01), mafic foidite (FS02), damtjernite (FS04, FS12, FS13), phonolite (FS07, FS08, FS09) and FDC (FS15, FS16), and six samples from the baked contact/host rocks at FS01, FS04, FS11, FS12 and FS13. Hysteresis loops for most of the specimens are narrow and saturated at an applied field of 500–1,000 mT, after correcting for paramagnetic contributions (Figure S11 in Supporting Information S1), and are consistent with pseudo-single domain (PSD) or multi-domain (MD) magnetite according to a Day plot (Figure 5a). The exceptions to this are samples interpreted to contain significant pyrrhotite (FS09I1, FS12K1) or hematite (FS15G1, FS16C1, FS11L1), based on their thermal remanence behavior.

Backfield curves generally saturate below 200 mT, with the exception of the aforementioned containing pyrrhotite (saturating up to 600 mT) or hematite (not fully saturated at 1.5 T). Unmixing of the backfield curves revealed three populations of unmixed components, UC1-UC3 (Figure 5b), with coercivity peaks at 3–22 mT (UC1), 19–74 mT (UC2) and 163–525 mT (UC3). Examples are shown in Figures 5c–5f) and Figures S12a–S12f in Supporting Information S1.

Thermal susceptibility curves are also consistent across the Fen complex, with most samples showing a flat response between 0 and 570°C and sudden decreases in susceptibility during heating between 570 and 600°C (Figures S10a-S10d in Supporting Information S1), consistent with magnetite. Significant Hopkinson peaks were not observed, suggesting that susceptibility is dominated by PSD or MD magnetite (Dunlop, 1974). Between 600 and 700°C, curves are generally flat, indicating minimal hematite, although a few showed minor drops around 680–690°C (Figure 5f, Figure S10e in Supporting Information S1). Susceptibility behavior during cooling was generally reversible, although some samples presented broad non-reversible peaks around 200–400°C during cooling (Figure S10c in Supporting Information S1) or heating (Figure S10f in Supporting Information S1).

Low-temperature data from the MPMS show magnetite Verwey transitions around 120 K (Figures 5c and 5d), and in a few cases there is evidence of a Besnus transition around 30–35 K, indicating the presence of pyrrhotite (Figure 5e), or a smeared Morin transition around 250–260 K, indicating hematite (Figure 5f). Where they could be obtained, FORC diagrams for samples containing component B display a broad distribution consistent with PSD particles (Figure 5c), while one sample containing component C showed a sharp ridge, consistent with non-interacting SD particles (Figure 5d).

4.4. Scanning Electron and Magnetic Microscopy

4.4.1. SEM-EDS Observations

Scanning electron microscopy (SEM) and elemental EDS mapping of thin sections from a damtjernite (FS04) revealed the presence of various magnetites in sizes ranging from submicron massive grains, up to large titanomagnetites 100s of microns in size (Figure 6d). These grains often exhibit clear trellis structures indicative of titanomagnetite which experienced oxy-exsolution at high temperature, usually rounded and significantly exsolved. Samples from a phonolite (FS09) and mafic foidite (FS02) revealed no visible magnetites, with the exception of those identified in Figure 7d. Fe-sulfides (mainly pyrrhotite, variably also pyrite), sphalerite, chalcopyrite, and barite were also present in all observed samples.

Figure 3. Representative Zijderveld (1967) diagrams for specimens containing components A (green), B (red), C (blue) and D (orange) with remanence and stereonet plots inset. (a) FS04D1 unblocks component B below 555°C, then moves along a great circle toward component C, up to 590°C, before the direction randomizes (TH only). (b) FS13Q1 does the same between 550 and 570°C. (c) FS04N1 unblocks component B up to 350°C (TH after AF up to 150 mT), then stabilizes at component C between 440 and 560°C (random directions above 570°C not shown for clarity). (d) FS15G1 unblocks component B to 520°C (TH only), then stabilizes at component C between 540 and 580°C (random higher temperature steps not shown). (e) FS13C1 unblocks component C down to 25% of its initial remanence between 20 and 85 mT, and the remainder decays linearly to the origin between 520 and 565°C. (f) FS11M1 unblocks component D from 0 to 690°C, consistent with hematite, with drops at 550 and 580°C, consistent with low Ti-magnetite and magnetite.

15252027, 2026, 5, Downloaded from https://agupubs.onlinelibrary.wiley.com/doi/10.1029/2025GC012881, Wiley Online Library on [07/11/2026]. See the Terms and Conditions (https://onlinelibrary.wiley.com/terms-and-conditions) on Wiley Online Library for rules of use; OA articles are governed by the applicable Creative Commons License

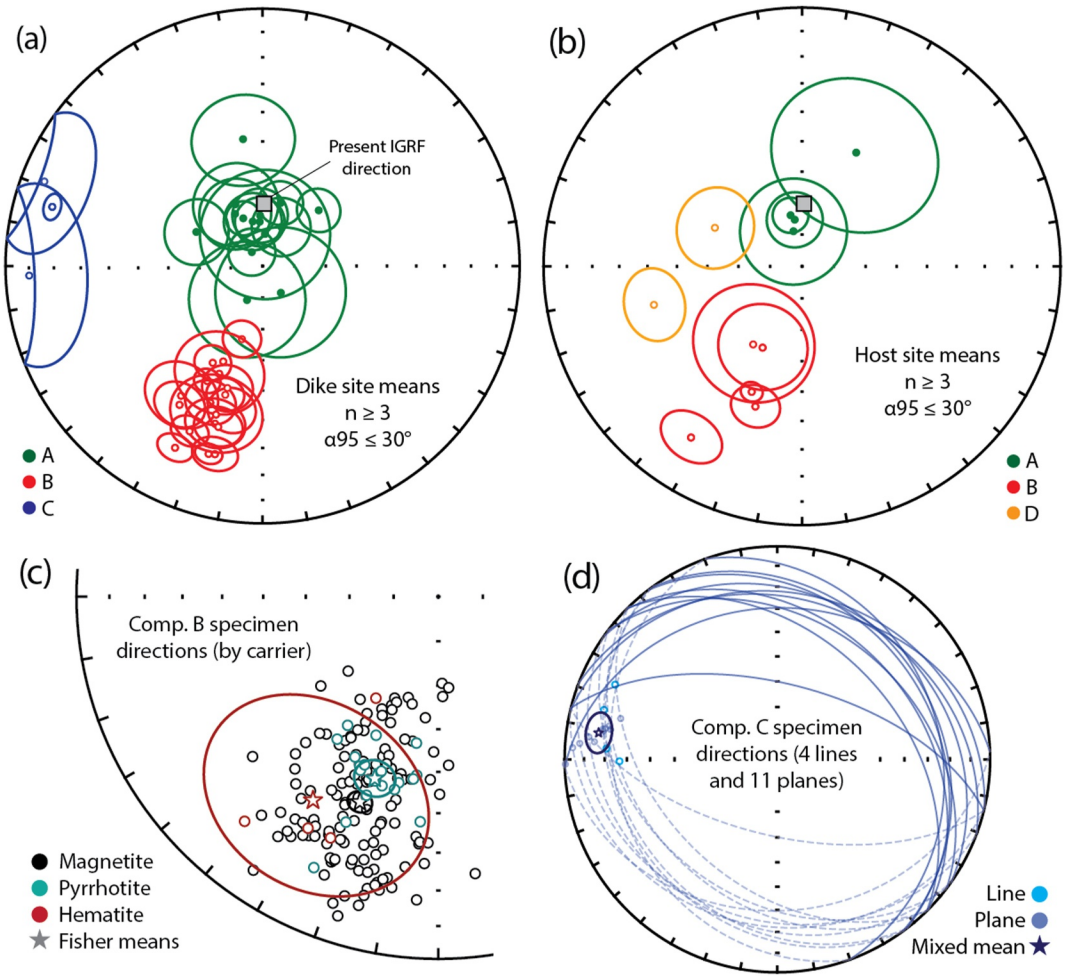


Figure 4. (a) Site mean directions for components A and B (dikes only), and C (dikes and contact zones). (b) Site mean directions for components A, B and D (host rocks only) derived from the contact tests (Figures S3–S9 in Supporting Information S1 Section D). (c) Specimen directions and means for component B (all rock types), distinguished by remanence carrier. Specimen means for magnetic, pyrrhotite and hematite overlap with the site mean directions for component B, suggesting they are all contemporaneous (Figures S1 and S2 in Supporting Information S1 Section C). (d) Specimen directions (lines and planes) for component C (all rock types) with a combined mean (McFadden & McElhinny, 1988).

4.4.2. QDM Observations

Micromagnetic maps were made on six thin sections from FS01 (diabase), FS02 (mafic foidite), FS04 (damtjernite), FS09 (phonolite) and FS15 (FDC). Thin sections were measured in an NRM state (Figures 6a and 7a), and then the same areas were measured again after applying IRM pulses ranging from 10 to 100 mT along the plane of the thin section (Figures 6b and 6c and 7b). Generally, dipoles coinciding with the positions of visible magnetites could be realigned with weak IRM fields of 10–15 mT, consistent with the behavior of multidomain (MD) magnetite (Figure 6b). However, some dipoles were not realigned by stronger fields (Figure 7b), indicating the presence of a higher coercivity remanence bearing phase, for example single-domain (SD) or pseudo-SD (PSD) magnetite or pyrrhotite. The locations of these dipoles were studied further with SEM-EDS to classify grain types. Two examples are given below.

4.4.3. FS04B4 (Damtjernite)

The NRM scan of FS04B4 showed many small dipoles with scattered orientations (Figure 6a). An IRM pulse of 10 mT was sufficient to realign most of the visible dipoles (Figure 6b), suggesting that these grains have low

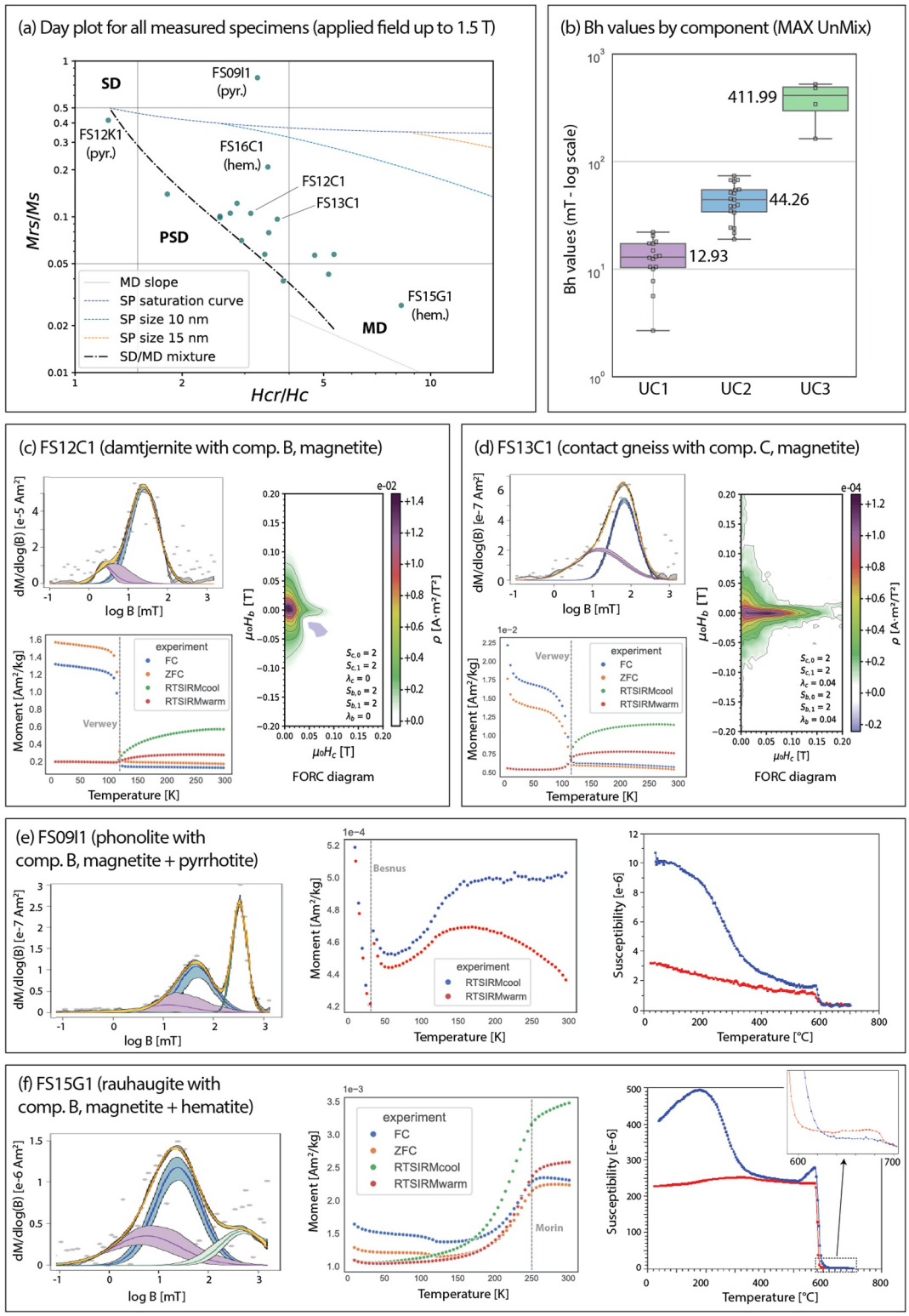


Figure 5. (a) Day plot for measured specimens. Most specimens plot near the SD/MD mixing line for titanomagnetite (Dunlop, 2002); those that plot elsewhere have significant contributions from hematite (hem.) or pyrrhotite (pyr.). (b) Coercivity values grouped by unmixed components UC1-UC3, based on unmixing of backfield curves with MAX UnMix (Maxbauer et al., 2016). (c, d) Unmixed backfield curves, MPMS experiments and FORC diagrams for FS12C1 (carrying component B) and FS13C1 (carrying component C). (e, f) Unmixed backfield curve, MPMS experiments and thermal susceptibility data for FS09I1 (with pyrrhotite) and FS15G1 (with hematite).

15252027, 2026, 5, Downloaded from https://agupubs.onlinelibrary.wiley.com/doi/10.1029/2025GC012881, Wiley Online Library on [07/11/2026]. See the Terms and Conditions (https://onlinelibrary.wiley.com/terms-and-conditions) on Wiley Online Library for rules of use; OA articles are governed by the applicable Creative Commons License

coercivities. At 22 mT (Figure 6c), all visible grains appear to be fully saturated (i.e., realigned and too strong to be accurately resolved with the QDM).

4.4.4. FS09A1 (Phonolite)

The NRM scan of FS09A1 (Figure 7a) showed only a weak remanence inside a large biotite book (ca. 250 × 250 μm). The surrounding matrix is free of visible dipoles (i.e., remanence-bearing grains). After an IRM pulse of 48 mT, the biotite grain still contained the only observable signal in the field of view (Figure 7b). Moreover, dipoles stemming from the biotite did not realign with the applied field, indicating a magnetic phase with a higher coercivity (e.g., SD magnetite or pyrrhotite). Detailed SEM mapping showed concentrations of very fine (<1 μm) interstitial magnetite in the cracks of the biotite (Figure 7c), which align with the dipoles mapped by the QDM, as well as small (<10 μm) scattered grains of sphalerite, ilmenite, galena and rutile (Figure 7d) not associated with dipoles. The dipoles mapped with the QDM appear to align with the highest concentrations of magnetite (Figures 7b and 7c).

5. Discussion

5.1. Interpretation of Components

Paleomagnetic directions derived from components B and C are presented in Figure 8a, alongside previous paleomagnetic results from Fen and Alnö. The corresponding poles are presented in Table 2 and Figures 8b and 8c. The component B pole is calculated by first converting the site means to VGPs and then taking the Fisher (1953) mean, while the component C pole is calculated using the method of McFadden and McElhinny (1988) in pole space (see Section 4.2.3). The interpretation of these components and comparison with previously published poles are discussed below.

5.1.1. Component A (Present Day Overprint)

Component A overlaps with the expected present-day field at the Fen complex (Figure 4a), and appears in all rock types (Table S5 in Supporting Information S1). The component has a low coercivity (<20 mT) and unblocks at low temperatures, generally <300°C, consistent with viscous behavior of large MD titanomagnetites (Butler, 1992). We interpret component A to be a viscous overprint formed in recent/present-day field conditions. We assign this component to UC1 in the backfield unmixing analysis (Figure 5b), with peak coercivities of 10–20 mT, and to large titanomagnetites observed in the QDM and SEM scans (e.g., Figure 6), containing dipoles which realigned in weak fields (<22 mT).

5.1.2. Component B (Permian Overprint)

Component B is also ubiquitous, being found in the Ediacaran intrusions, as well as younger diabase intrusions (FS01 and FS18). Within 4 km of the main complex, component B is also found in the Mesoproterozoic host rocks, up to 20 m away from the intrusions, resulting in negative contact tests. Further away (10–25 km from the main complex), contact tests on the Fen intrusions were inconclusive, although at FS12 and FS14, component B is also present in the fenitisation halos (within 35 cm of the intrusions). The component is carried mainly by magnetite (unblocking below 550–580°C or below 60 mT), consistent with population UC2 in the backfield unmixing curves (Figure 5b), with peak coercivities of 30–45 mT, indicating PSD magnetite and grain sizes of ca. 0.05–10 micron (Dunlop, 2002). In some cases, component B is also carried by hematite, unblocking up to 690°C with TH demagnetization (Figure 2f), or pyrrhotite, unblocking between 300 and 350°C with TH following AF demagnetization (Figures 2e and 3c), consistent with population UC3 in the backfield unmixing curves (Figure 5b).

15252027, 2026, 5, Downloaded from https://agupubs.onlinelibrary.wiley.com/doi/10.1029/2025GC012881, Wiley Online Library on [07/11/2026]. See the Terms and Conditions (https://onlinelibrary.wiley.com/terms-and-conditions) on Wiley Online Library for rules of use; OA articles are governed by the applicable Creative Commons License

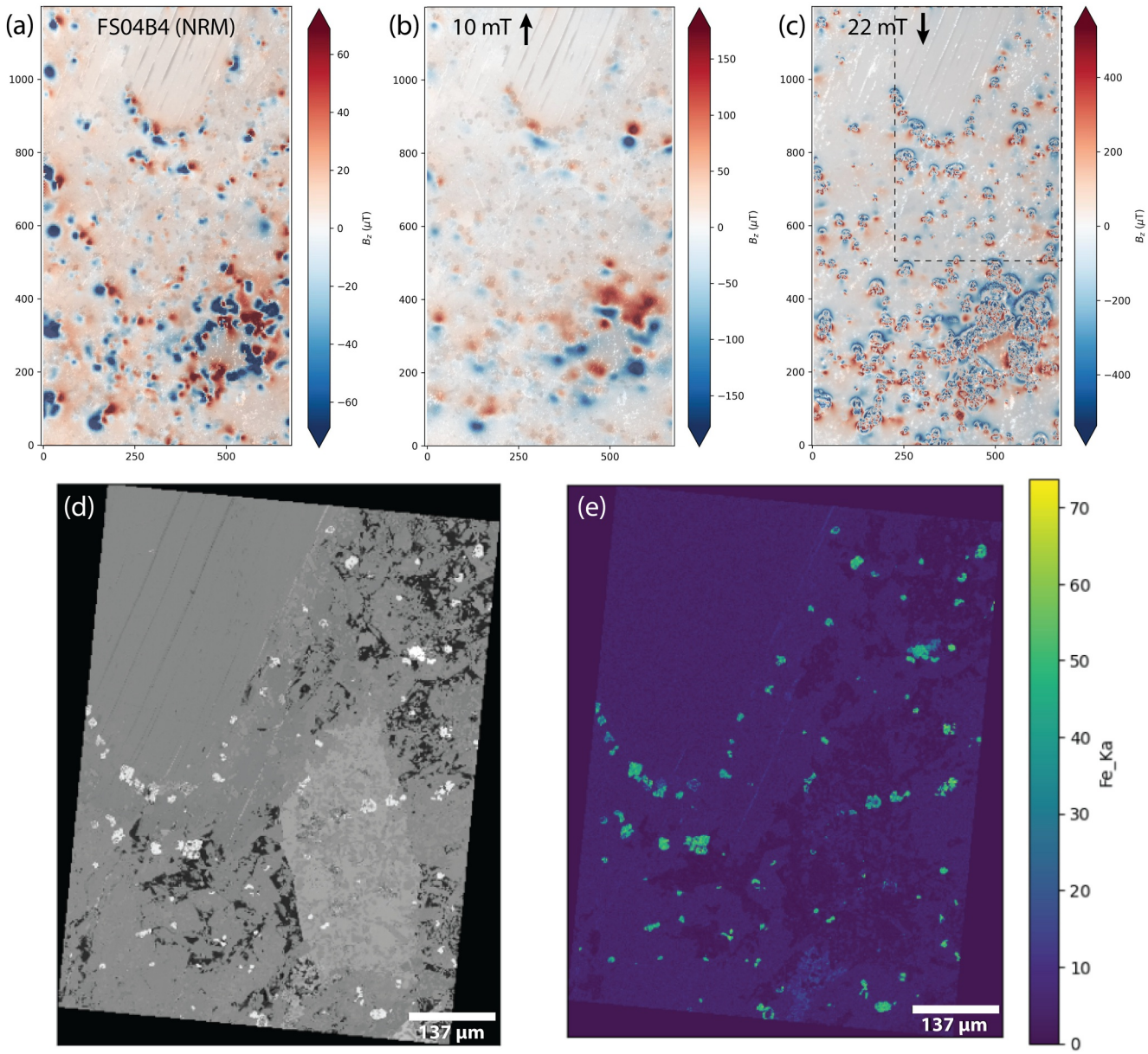


Figure 6. QDM scans of a thin section from FS04B4 (a) before and after applying IRM pulses of (b) 10 mT (up in the plane of the image) and (c) 22 mT (down). The *x*-*y* axes are in pixels which are equivalent to ca. 1 μm. (d, e) Back-scatter electron (BSE) image and Fe map (arbitrary units) for area of interest marked up in panel (c). Strong dipoles with weak coercivities appear to be associated with large (10–50 μm) titanomagnetite grains which are completely saturated at 22 mT. Note that in panel (c) we only interpret the general orientation of the measured dipoles, as the sharp magnetic gradients observed are likely artifacts arising from saturation of the QDM.

Directions from component B appear in only one polarity (Figure 4a) and the corresponding pole (derived from dike site means) lies on Baltica's APWP at ca. 270 Ma (Figure 8b), indicating a secondary nature. This timing is consistent with the age of the nearby Oslo Rift and Permo-Carboniferous intrusions which are found in the Fen complex and surrounding areas. Moreover, the reversed polarity is consistent with the Kiaman reversed superchron ca. 320-250 Ma (Courtillot & Besse, 1987), assuming Baltica was in the northern hemisphere at that time (Torsvik & Cocks, 2017). Meert et al. (1998) showed their mean Fen direction to be slightly shallower than directions found in Oslo Rift rocks and suggested that the similarity in directions could be coincidental. However, our component B mean is essentially identical to the directions recently found in Oslo Rift rocks (Dominguez et al., 2011; Haldan et al., 2014; Figure 8b). We therefore conclude that component B is a secondary magnetisation acquired ca. 270 Ma. We note that the component B directions from some damtjernites (e.g., FS04 and

15252027, 2026, 5, Downloaded from https://agupubs.onlinelibrary.wiley.com/doi/10.1029/2025GC012881, Wiley Online Library on [07/11/2026]. See the Terms and Conditions (https://onlinelibrary.wiley.com/terms-and-conditions) on Wiley Online Library for rules of use; OA articles are governed by the applicable Creative Commons License

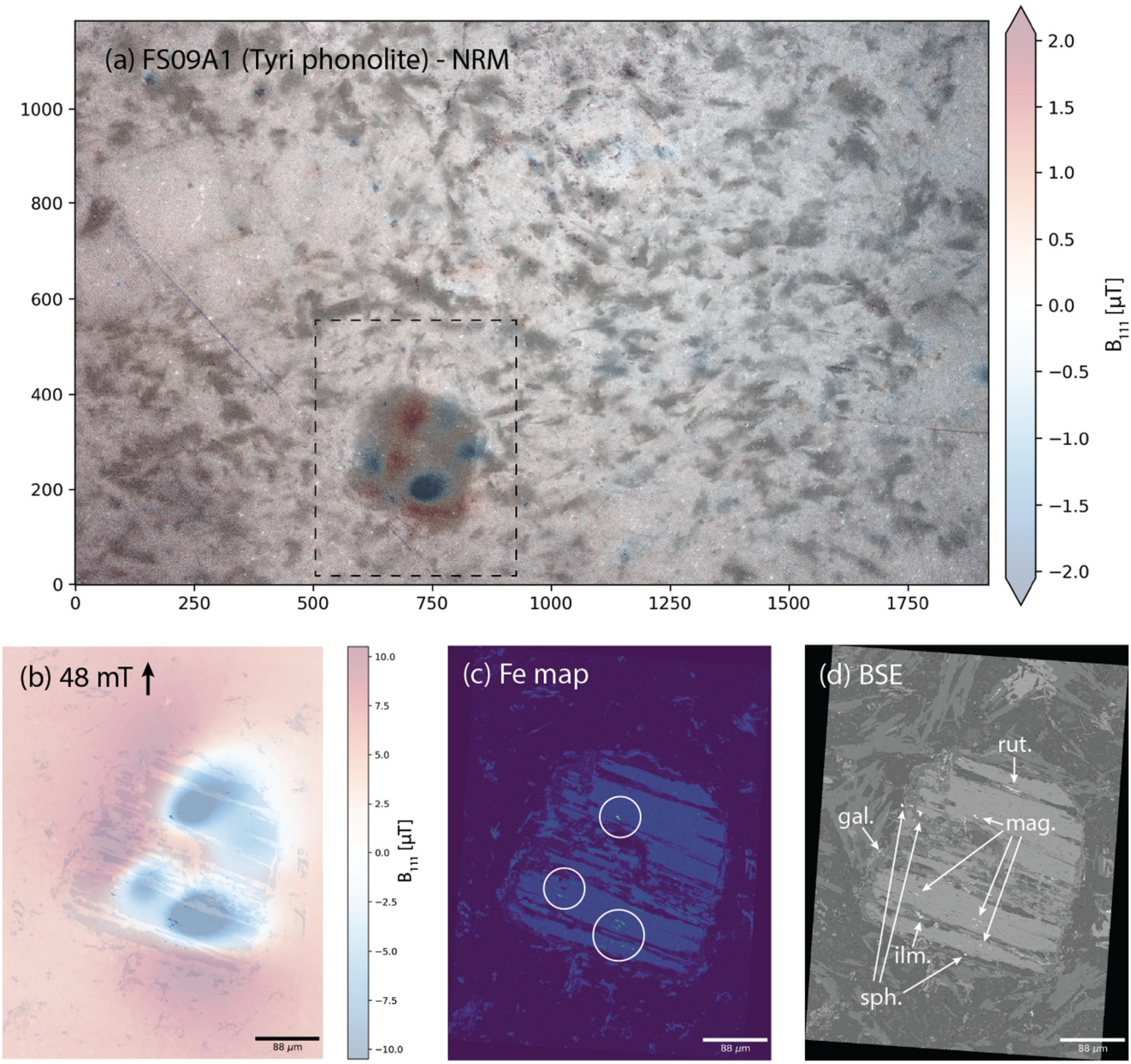


Figure 7. QDM scans of a biotite grain (a) before and (b) after applying an IRM pulse of 48 mT (up in the plane of the image). The only observed dipoles occur within the biotite grain, which did not realign with a strong IRM. (c, d) Fe element map and BSE image of the biotite. The three observed dipoles in panels (a, b) appear to be associated with fine-grained (<1 μm) interstitial magnetite (mag.). The other electrodense grains are sphalerite (sph.), ilmenite (ilm.), galena (gal.) and Fe-bearing rutile (rut.), which do not appear to be remanence carriers but may indicate low-temperature alteration.

FS13) are significantly shallower than in the host rocks (Figures S4 and S5 in Supporting Information S1). We attribute this to a greater influence of component A and overlapping coercivity spectra within the intrusions, effectively "smearing" the B direction toward the A direction; this interpretation is supported by strong great circle behavior between the components, implying that component B is not fully resolved by PCA in these cases, resulting in spurious shallow directions (Dinarès-Turell & McClelland, 1991; Tonti-Filippini & Gilder, 2023).

The presence of pyrrhotite as a remanence carrier may indicate that the Fen complex is within the contact aureole of the Permian intrusives (Antun, 1967). Support for this conclusion can also be found in the paleomagnetic records of younger rocks of the Oslo Rift. Dominguez et al. (2011) conducted a paleomagnetic study of the ca. 270 Ma Lunner dykes and their host rocks (which included early Paleozoic carbonates and earlier Permian

15252027, 2026, 5, Downloaded from https://agupubs.onlinelibrary.wiley.com/doi/10.1029/2025GC012881, Wiley Online Library on [07/11/2026]. See the Terms and Conditions (https://onlinelibrary.wiley.com/terms-and-conditions) on Wiley Online Library for rules of use; OA articles are governed by the applicable Creative Commons License

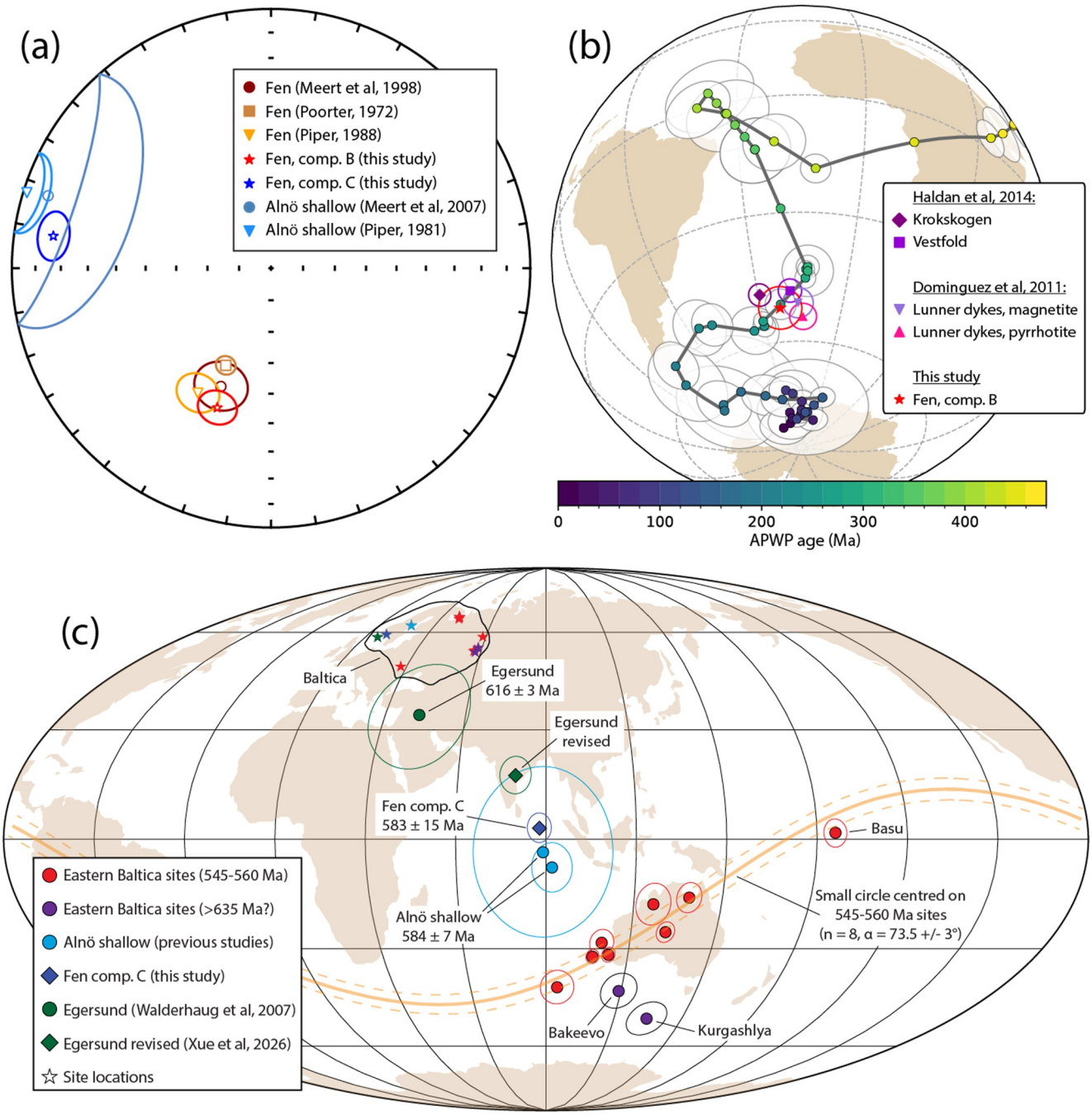


Figure 8. (a) Mean directions for components B and C (this study) alongside results from previous paleomagnetic studies of Fen and Alnö (in geographic coordinates). (b) The pole derived from component B lies on Baltica's APWP (Torsvik et al., 2012) at 270 Ma, and overlaps with poles recently derived from Permian rocks in the Oslo Rift (Dominguez et al., 2011; Haldan et al., 2014). (c) The Fen component C pole (this study) lies far from the APWP and overlaps with the Alnö shallow poles of Meert et al. (2007) and Piper (1981), and close to the revised Egersund pole of Xue et al. (2026). The 545–560 Ma poles from Eastern Baltica are distributed on a small circle centered on the sample sites, which suggests that their distribution may be affected by vertical axis rotations. The poles from Bakeevo and Kurgashlya have uncertain ages and could be pre-Ediacaran (see main text). All relevant poles are listed in Table S6 in Supporting Information S1.

igneous rocks) in the Oslo region and found that the host rocks invariably carried the same magnetic direction as the Lunner dykes, even at distances "where they could not have been thermally remagnetized by the intrusive event". Moreover, those authors reported a widespread occurrence of pyrrhotite, which they inferred to be a major carrier of a chemical remagnetization, likely as a result of hydrothermal fluid circulation. We observe that our

15252027, 2026, 5, Downloaded from https://agupubs.onlinelibrary.wiley.com/doi/10.1029/2025GC012881, Wiley Online Library on [07/11/2026]. See the Terms and Conditions (https://onlinelibrary.wiley.com/terms-and-conditions) on Wiley Online Library for rules of use; OA articles are governed by the applicable Creative Commons License

15252027, 2026, 5, Downloaded from https://agupubs.onlinelibrary.wiley.com/doi/10.1029/2025GC012881, Wiley Online Library on [07/11/2026]. See the Terms and Conditions (https://onlinelibrary.wiley.com/terms-and-conditions) on Wiley Online Library for rules of use; OA articles are governed by the applicable Creative Commons License

Table 2
Poles Derived From Components B and C (This Study), Compared to Previous Results From Fen and Alnö

Location (reference)	N	λ_P	ϕ_P	A_{95}	Age (Ma)	Note
Fen (Meert et al., 1998)	6	56	150	8.4	583 ± 15	D_p/D_m = 7/10
Fen (Piper, 1988)	26	50.1	143.9	6.2		D_p/D_m = 4.9/7.9
Fen (Poorter, 1972)	19	63	142	3.5		D_p/D_m = 3/4
Fen comp. B (this study)	17	52.9	156.6	4.9		site mean
Fen comp. C (this study)	15	−1.7	266.6	4.5		specimen mean
Alnö (Meert et al., 2007)	6	3.5	269	23.2	584 ± 7	D_p/D_m = 16.5/32.5
Alnö (Piper, 1981)	21	7.6	272	6.7		D_p/D_m = 5/9

Note. N = number of sites (or specimens). λ_P/ϕ_P = pole latitude/longitude (°N/°E). For the older studies, A_{95} (°) is estimated by $\sqrt{D_p * D_m}$ (Khramov, 1987).

component B (which is also partly carried by pyrrhotite) is quite similar to the pyrrhotite remanence reported by Dominguez et al. (2011), which they inferred was acquired between 271 and 267 Ma.

We speculate that hydrothermal fluids associated with the rifting event reactivated the Fen's ancient plumbing system and pervasively altered all associated intrusions, as well as the fenitised host rocks within the main complex and halos adjacent to the satellite dikes. Supporting this, QDM and SEM-EDS analyses of the Tyri phonolite (FS09), also sampled by Meert et al. (1998), showed the high-coercivity (>48 mT) dipoles to be associated with a biotite grain. This biotite is interpreted as an antecryst which was resorbed at magmatic temperatures. It is not clear whether the magnetite, rutile and ilmenite, which occur along the biotite basal cleavage inside the biotite grain (Figure 7d), formed at this stage or during later hydrothermal activity. However, the presence of sphalerite and galena nearby suggests that both magmatic and hydrothermal processes produced the observed minerals. We were unable to locate/isolate the high-coercivity magnetites in the FS04 damtjernite, as the QDM signal was overwhelmed by dipoles associated with low-coercivity magnetite. The high-coercivity magnetites could also be too small to observe given the QDM's resolution (i.e., <1.2 μm). All visible magnetites in FS04 appear to be altered, but this could be a consequence of submagmatic processes during initial cooling, and not necessarily related to later hydrothermal activity. Nonetheless, the fenitised contact rock adjacent to FS04 shows signs of secondary alteration (Section A in Supporting Information S1), further supporting our hydrothermal interpretation.

5.1.3. Component C (Primary Ediacaran Direction)

Component C appears only during thermal demagnetization, suggesting that it has a coercivity range similar to, or lower than, components A and B. Component C is extremely weak, often <5% of the initial NRM, and is mainly found where component B unblocks at lower temperatures (ca. 550°C), perhaps establishing an unblocking "window" where a weaker, higher-order component can be observed (Dunlop, 1979). This interpretation is supported by progressive movement from B to C along a great circle observed in many samples, indicative of superimposed unblocking spectra where a CRM (chemical remanent magnetisation) overprint partially overlaps a primary component (Schwarz & Buchan, 1989). As component C randomizes above 590°C, it is likely also carried by fine-grained magnetite. The prevalence of component C in the contact zones (e.g., Figures 3c and 3e) may be due to the component in the host rock being a TRM (thermal remanent magnetisation) and therefore more resistant to AF, as a CRM in magnetite should easier to remove with AF (Schmidt, 1993).

The shallow directions of component C may finally resolve the discrepancies between the paleomagnetic records from Fen and Alnö. The pole derived from component C (Figure 8c) is unique from any younger poles from Baltica, supporting a primary nature. At Fen, component C only appears in one polarity, however its corresponding pole overlaps with the "Alnö shallow" pole (Figure 8a), which is defined by dual-polarity directions. We therefore interpret component C to be primary, although its corresponding pole is of relatively low quality, scoring 4 (out of 7) on the quality index of Meert et al. (2020), due to the low number of sites/samples containing the component, a lack of positive field tests, and absence of reversals. We assign our pole an age of 583 ± 15 Ma, as derived by Meert et al. (1998), although we recognize that the biotite and phlogopite dates could be affected by Ar loss due to fluid

15252027, 2026, 5, Downloaded from https://agupubs.onlinelibrary.wiley.com/doi/10.1029/2025GC012881, Wiley Online Library on [07/11/2026]. See the Terms and Conditions (https://onlinelibrary.wiley.com/terms-and-conditions) on Wiley Online Library for rules of use; OA articles are governed by the applicable Creative Commons License

interaction, and that the true emplacement age could be older than 583 Ma; further geochronological and thermochronological data for the complex would be useful to clarify this. A more detailed study of the directions in the Alnö complex may yield a higher quality pole, due to the relative abundance of sites containing the shallow component, the presence of reversals, and opportunities to obtain definitive baked contact tests.

The source of component C is still obscure and we were unable to resolve it with QDM/SEM analyses of specimens from Fen. At both Fen and Alnö, the occurrence of a shallow component is rare and seems bound to particular rock types (mainly damtjernites in Fen, søvites and alnöites in Alnö). More detailed magnetic microscopy investigations, coupled with SEM measurements, may be able to tease out the primary remanence carriers of the shallow component. We suspect that it is carried by primary nanoscopic inclusions of magnetite in grains capable of shielding it from later alteration, for example, garnet (Brearley & Champness, 1986), pyroxene (Feinberg et al., 2005), or some other chemically resistant phase. This is supported by the FORC diagram of sample FS13C1, which indicates the presence of SD magnetite (Figure 5d). The contact zones may be better at shielding these weak primary components from later fluids, which can more easily permeate the intrusions (e.g., Xue et al., 2026). However, the example from the FS04 damtjernite contact zone shows that the fenitised zone in the wall-rock adjacent to the dike margin has also been post-magmatically altered (Section A in Supporting Information S1).

5.1.4. Component D (Early Neoproterozoic Metamorphism)

Component D only appears in the host rocks at two sites (FS11 and FS14) and decays unidirectionally to the origin, carried by both magnetite and hematite according to TH demagnetization (Figure 3f). This behavior suggests the component is a product of high-temperature metamorphism, consistent with our understanding of quartzites from the Telemarkia terrane, which experienced high-temperature metamorphism ca. 930-920 Ma (Bingen et al., 2008). Supporting this interpretation, the direction of component D is similar to mid-inclination westerly directions found in metamorphic rocks of the nearby Modum Complex (Jensen, 2017; Robinson et al., 2014). We interpret component D to have been acquired during metamorphism in the Early Neoproterozoic and therefore to be older than the Ediacaran intrusions. The survival of this component further reinforces that remagnetization of Fen was a spatially restricted phenomenon that exploited the existing plumbing system of the complex and its satellite intrusions.

5.2. Comparison With Ediacaran Poles From Baltica

Figure 8c shows the new Fen pole, derived from component C, alongside other poles from Baltica, where all poles are displayed in the same hemisphere to minimize travel on the apparent polar wander path (APWP). Our pole plots close to a revised pole from the Egersund dikes ca. 616 ± 3 Ma (Xue et al., 2026), and indicates that Baltica was at low/equatorial latitudes ca. 583 Ma. This differs slightly to the younger (545–560 Ma) poles from eastern Baltica, which are significantly dispersed. We note that these poles are distributed on a small circle centered on their sampling sites, suggesting they formed at similar paleolatitudes and that vertical axis rotations may play a role in their dispersion, as also noted by Meert (2014). Furthermore, a prominent outlier from the Basu formation overlaps Baltica's APWP at 450-440 Ma, so the possibility of remagnetization cannot be ruled out, as recognised by Golovanova et al. (2011). However, interrogation of these inferences is beyond the scope of our study.

We have excluded two poles listed by Domeier et al. (2023), Bakeevo and Kurgashlya, because they have questionable ages and may be pre-Ediacaran. Lubnina et al. (2014) assigned ages of ca. 570–600 Ma to these poles, based on the interpretation of Puchkov (2012). However, Zaitseva et al. (2019) dated the Bakeevo Formation to 642 ± 9 Ma, based on Rb-Sr dating of glauconite, and Środoń et al. (2022) correlated the Kurgashlya formation with the Arsha group, which contains effusive rocks with zircons U-Pb dated to 709.9 ± 7.3 Ma. If the previously published Fen and Alnö steep poles are also excluded, the remaining Ediacaran poles for Baltica show a slow progression in paleolatitude between 616–545 Ma (Figure 8c), although there is unresolved scatter among the poles from eastern Baltica.

The weak and obscure nature of component C is consistent with paleointensity estimates of the late Ediacaran paleomagnetic field (Huang et al., 2024; Thallner et al., 2021), and our preferred interpretation is that Baltica occupied low to moderate latitudes under a dominantly dipolar, albeit relatively weak, field at this time. This view contrasts with several mid-to late- Ediacaran records from other continents, particularly Laurentia and Northwest Africa, that have been interpreted to reflect large, rapid polar wander events or substantial departures from an

15252027, 2026, 5, Downloaded from https://agupubs.onlinelibrary.wiley.com/doi/10.1029/2025GC012881, Wiley Online Library on [07/11/2026]. See the Terms and Conditions (https://onlinelibrary.wiley.com/terms-and-conditions) on Wiley Online Library for rules of use; OA articles are governed by the applicable Creative Commons License

axial dipole field, even though many of these data sets are sparse, may contain mixed or overprinted components, or derive from units with complex tectono-thermal histories (Domeier et al., 2023). Our new pole from the Fen complex suggests that the Baltica data set does not require such exotic explanations, highlighting both the current limitations of the global Ediacaran paleomagnetic database and the need for additional high-quality, well-dated studies before a fully consistent picture of geomagnetic field behavior and plate motions can be established for this interval.

6. Conclusions

Our study of the Fen complex revealed four paleomagnetic components which we interpret as follows:

1. Component A is a viscous overprint acquired in recent/present-day geomagnetic field conditions. The component is carried by large titanomagnetite grains with low coercivites (<20 mT), which is supported by our rock magnetic measurements (backfield remanence and thermal susceptibility curves) and SEM/QDM observations.
2. Component B is a CRM acquired during the Permian (ca. 270 Ma), due to hydrothermal fluids (<300°C) permeating the complex and its satellite intrusions during the formation of the Oslo Rift. The component is carried by fine-grained (submicron) PSD magnetite with coercivities of 20–60 mT, based on its thermal and AF demagnetization behavior and unmixing of backfield curves. In several instances, the component is also carried by pyrrhotite and hematite. In a phonolite (FS09), high-coercivity magnetite is associated with biotite grains and occurs interstitially alongside other low-temperature alteration products (sphalerite, galena and ilmenite), inferred from QDM/SEM observations.
3. Component C is a primary component acquired during formation of the Fen complex (ca. 583 Ma). The component is also carried by fine-grained magnetite, based on its thermal remanence behavior and susceptibility curves; the FORC diagram of a contact sample from FS13 suggests that the component is carried by SD magnetite. A primary nature of component C is supported by its similarity to the shallow directions from the Alnö complex which have dual-polarity and are distinct from any younger directions from Baltica.
4. Component D was acquired during metamorphism of the Telemarkia terrane ca. 930-920 Ma. The component is present in Late Mesoproterozoic/Early Neoproterozoic quartzite and granitic gneiss outside of the main complex, beyond the fenitisation halos, and is a TRM carried by magnetite and hematite. The survival of this component reinforces that remagnetization of the Fen complex was spatially restricted, which implies exploitation of its plumbing by fluids.

Our new pole for the Fen complex, derived from component C, places Baltica at low/equatorial latitudes ca. 583 Ma. A comparison of our pole with other data from Baltica supports a GAD field and a slow and progressive APWP from 616 to 545 Ma, which is currently at odds with findings from other continents.

Conflict of Interest

The authors declare no conflicts of interest relevant to this study.

Availability Statement

The paleomagnetic data used in this study are publicly available in the MagIC database via Tonti-Filippini et al. (2026).

Acknowledgments

MD and JT conceived the idea for this study, with significant guidance from SD. JT, SD, PA and PS carried out sampling in 2023–2025. Sampling site selection and petrography by SD. Paleomagnetic and rock magnetic experiments by JT and PA. QDM observations by RdB and BdG, coordinated by LdG, with analyses by JT and LG. SEM observations performed by JT, with significant input from SD and LG. JT wrote the manuscript with significant input from the other authors. Funding was provided by the ERC Consolidator Grant "Untangling Ediacaran Paleomagnetism to Contextualize Immense Global Change" (EPIC; project no. 101043844) and the Research Council of Norway, through its Centres of Excellence funding scheme (Centre for Planetary Habitability; project no. 332523). We thank Statens naturoppsyn (SNO) and local landowners for access to the sampling sites, and Yi Xue, Annique van der Boon, Petr Gromov, and Margrethe and Eva Onarheim for assistance with fieldwork. JT thanks Muriel Erambert and Siri Simonsen for assistance with microscopy, and Trond Torsvik for useful discussions. We also thank the editor, Sonia Tikoo, and two reviewers, Nicholas Swanson-Hysell and Daniel Pastor-Galán, for their suggestions which improved the manuscript.

References

Abrajevitch, A., & Van der Voo, R. (2010). Incompatible Ediacaran paleomagnetic directions suggest an equatorial geomagnetic dipole hypothesis. *Earth and Planetary Science Letters*, *293*(1–2), 164–170. https://doi.org/10.1016/j.epsl.2010.02.038

Agić, H., Jensen, S., Meinhold, G., Högström, A. E., Ebbestad, J. O. R., Høyberget, M., et al. (2024). Life through an Ediacaran glaciation: Shale- and diamictite-hosted organic-walled microfossil assemblages from the late Neoproterozoic of the Tanafjorden area, northern Norway. *Palaeogeography, Palaeoclimatology, Palaeoecology*, *635*, 111956. https://doi.org/10.1016/j.palaeo.2023.111956

Alken, P., Thébault, E., Beggan, C. D., Amit, H., Aubert, J., Baerenzung, J., et al. (2021). International Geomagnetic Reference Field: The thirteenth generation. *Earth Planets and Space*, *73*(1), 49. https://doi.org/10.1186/s40623-020-01288-x

Antun, P. (1967). Sedimentary pyrite and its metamorphism in the Oslo region. *Norsk Geologisk Tidsskrift*, *47*, 211–235.

Barth, T., & Ramberg, I. (1966). The Fen circular complex. In O. Tuttle & J. Gittins (Eds.), *Carbonatites* (pp. 225–257). J. Wiley and Sons.

Bingen, B., Davis, W. J., Hamilton, M. A., Engvik, A. K., Stein, H. J., Skar, O., & Nordgulen, O. (2008). Geochronology of high-grade metamorphism in the Sveconorwegian belt, S. Norway: U-Pb, Th-Pb and Re-Os data. *Norwegian Journal of Geology/Norsk Geologisk Forening*, *88*(1).

Bingen, B., Griffin, W. L., Torsvik, T. H., & Saeed, A. (2005). Timing of late Neoproterozoic glaciation on Baltica constrained by detrital zircon geochronology in the Hedmark Group, south-east Norway. *Terra Nova*, *17*(3), 250–258. https://doi.org/10.1111/j.1365-3121.2005.00609.x

Brearley, A., & Champness, P. (1986). Magnetite exsolution in almandine garnet. *Mineralogical Magazine*, *50*(358), 621–633. https://doi.org/10.1180/minmag.1986.050.358.07

Brenner, A. R., Fu, R. R., Kylander-Clark, A. R., Hudak, G. J., & Foley, B. J. (2022). Plate motion and a dipolar geomagnetic field at 3.25 Ga. *Proceedings of the National Academy of Sciences*, *119*(44), e2210258119. https://doi.org/10.1073/pnas.2210258119

Brøgger, W. C. (1921). Die Eruptivgesteine des Kristianiagebietes: Das Fengebiet in Telemark, Norwegen/von WC Brøgger. In *Kommission bei Jacob Dybwad*.

Buchan, K. L. (2007). Baked contact test. In *Encyclopedia of Geomagnetism and Paleomagnetism* (pp. 35–39). Springer.

Butler, R. F. (1992). *Paleomagnetism: Magnetic domains to geologic terrains*. Blackwell Scientific Publications.

Bylund, G., & Zellman, O. (1980). Palaeomagnetism of the dolerites of the Särv Nappe, southern Swedish Caledonides. *Geologiska Foreningen i Stockholm Forhandlingar*, *102*(4), 393–402. https://doi.org/10.1080/11035898009454496

Chadima, M. (2006). Remasoft 3.0 a user-friendly paleomagnetic data browser and analyzer. *Travaux Géophysiques*, *27*, 20.

Cogné, J. P. (2003). PaleoMac: A Macintosh™ application for treating paleomagnetic data and making plate reconstructions. *Geochemistry, Geophysics, Geosystems*, *4*(1), 2001GC000227. https://doi.org/10.1029/2001GC000227

Corfu, F., & Dahlgren, S. (2008). Perovskite U–Pb ages and the Pb isotopic composition of alkaline volcanism initiating the Permo-Carboniferous Oslo Rift. *Earth and Planetary Science Letters*, *265*(1–2), 256–269. https://doi.org/10.1016/j.epsl.2007.10.019

Courtillot, V., & Besse, J. (1987). Magnetic field reversals, polar wander, and core-mantle coupling. *Science*, *237*(4819), 1140–1147. https://doi.org/10.1126/science.237.4819.1140

Creer, K., Irving, E., & Runcorn, S. (1957). VI. Geophysical interpretation of palaeomagnetic directions from Great Britain. *Philosophical Transactions of the Royal Society of London. Series A, Mathematical and Physical Sciences*, *250*(974), 144–156. https://doi.org/10.1098/rsta.1957.0017

Dahlgren, S. (1987). *The satellitic intrusions in the Fen Carbonatite- Alkaline Rock Province, Telemark, Southeastern Norway. Distribution, emplacement, compositional characteristics and petrology. (Thesis)*. University of Oslo.

Dahlgren, S. (1994). Late Proterozoic and Carboniferous ultramafic magmatism of carbonatitic affinity in southern Norway. *Lithos*, *31*(3–4), 141–154. https://doi.org/10.1016/0024-4937(94)90005-1

Dahlgren, S. (2019). REE mineralization in the Fen Carbonatite Complex, Telemark, Norway—A world-class exploration target for the Hi-Tech and "Green-shift" industry? (Tech. Rep.). *Buskerud Telemark Vestfold County Councils*. Retrieved 2025-12-19, from https://www.telemarkfylke.no/globalassets/tfk/dokumenter/regiongeologen/2019_11_17_fen_ree_resources_geoladvisor_sdahlgren_final24_small.pdf

de Oliveira, W. P., Hartmann, G. A., Terra-Nova, F., Brandt, D., Biggin, A. J., Engbers, Y. A., et al. (2021). Paleosecular variation and the time-averaged geomagnetic field since 10 Ma. *Geochemistry, Geophysics, Geosystems*, *22*(10), e2021GC010063. https://doi.org/10.1029/2021GC010063

de Wall, H., & Greiling, R. (2000). Remagnetisation and magnetic refraction in Proterozoic dykes from Central Scandinavia during Caledonian deformation. *Physics and Chemistry of the Earth - Part A: Solid Earth and Geodesy*, *25*(5), 519–524. https://doi.org/10.1016/S1464-1895(00)00080-6

Dietzel, C. A., Kristandt, T., Dahlgren, S., Giebel, R. J., Marks, M. A., Wenzel, T., & Markl, G. (2019). Hydrothermal processes in the Fen alkaline-carbonatite complex, southern Norway. *Ore Geology Reviews*, *111*, 102969. https://doi.org/10.1016/j.oregeorev.2019.102969

Dinarès-Turell, J., & McClelland, E. (1991). A cautionary tale for palaeomagnetists: A spurious apparent single component remanence due to overlap of blocking-temperature spectra of two components. *Geophysical Research Letters*, *18*(7), 1297–1300. https://doi.org/10.1029/91GL01335

Domeier, M., Robert, B., Meert, J. G., Kulakov, E. V., McCausland, P. J., Trindade, R. I., & Torsvik, T. H. (2023). The enduring Ediacaran paleomagnetic enigma. *Earth-Science Reviews*, *242*, 104444. https://doi.org/10.1016/j.earscirev.2023.104444

Dominguez, A. R., Van der Voo, R., Torsvik, T. H., Hendriks, B. W., Abrajevitch, A., Domeier, M., et al. (2011). The 270 Ma palaeolatitude of Baltica and its significance for Pangea models. *Geophysical Journal International*, *186*(2), 529–550. https://doi.org/10.1111/j.1365-246X.2011.05061.x

Dunlop, D. J. (1974). Thermal enhancement of magnetic susceptibility. *Journal of Geophysics*, *40*(1), 439–451.

Dunlop, D. J. (1979). On the use of Zijderveld vector diagrams in multicomponent paleomagnetic studies. *Physics of the Earth and Planetary Interiors*, *20*(1), 12–24. https://doi.org/10.1016/0031-9201(79)90103-1

Dunlop, D. J. (2002). Theory and application of the Day plot (Mrs/Ms versus Hcr/Hc) 1. Theoretical curves and tests using titanomagnetite data. *Journal of Geophysical Research*, *107*(B3), EPM–4. https://doi.org/10.1029/2001JB000486

Evans, D. A. (2006). Proterozoic low orbital obliquity and axial-dipolar geomagnetic field from evaporite palaeolatitudes. *Nature*, *444*(7115), 51–55. https://doi.org/10.1038/nature05203

Fedorova, N., Levashova, N., Meert, J., Maslov, A., & Krupenin, M. (2014). New paleomagnetic data on Baltica based on upper Ediacaran deposits on the western slope of the Middle Urals. In *Doklady Earth Sciences* (Vol. 456(1), pp. 512–516). Springer. https://doi.org/10.1134/S1028334X14050134

Feinberg, J. M., Scott, G. R., Renne, P. R., & Wenk, H.-R. (2005). Exsolved magnetite inclusions in silicates: Features determining their remanence behavior. *Geology*, *33*(6), 513–516. https://doi.org/10.1130/G21290.1

Fisher, R. A. (1953). Dispersion on a sphere. *Proceedings of the Royal Society of London. Series A. Mathematical and Physical Sciences*, *217*(1130), 295–305. https://doi.org/10.1098/rspa.1953.0064

Fredrichsen, H. (1968). Sauerstoffisotopen einiger Minerale der Karbonatite des Fengebietes, Süd Norwegen. *Lithos*, *1*(1), 70–75. https://doi.org/10.1016/S0024-4937(68)80036-2

Gee, D. G., Juhlin, C., Pascal, C., & Robinson, P. (2010). Collisional orogeny in the Scandinavian Caledonides (COSC). *GFF*, *132*(1), 29–44. https://doi.org/10.1080/11035891003759188

Glenn, D. R., Fu, R. R., Kehayias, P., Le Sage, D., Lima, E. A., Weiss, B. P., & Walsworth, R. L. (2017). Micrometer-scale magnetic imaging of geological samples using a quantum diamond microscope. *Geochemistry, Geophysics, Geosystems*, *18*(8), 3254–3267. https://doi.org/10.1002/2017GC006946

Golovanova, I., Danukalov, K., Kozlov, V., Puchkov, V., Pavlov, V., Gallet, Y., et al. (2011). Paleomagnetism of the Upper Vendian Basu formation of the Bashkirian Meganticlinorium revisited. *Izvestiya, Physics of the Solid Earth*, *47*(7), 623–635. https://doi.org/10.1134/S1069351311070020

Gong, Z., Evans, D. A., Fu, R. R., & Xu, S. (2025). Reassessing the geocentric-axial-dipole (GAD) model for Proterozoic time with paleomagnetic directions from dike swarms. *Earth and Planetary Science Letters*, *667*, 119508. https://doi.org/10.1016/j.epsl.2025.119508

15252027, 2026, 5, Downloaded from https://agupubs.onlinelibrary.wiley.com/doi/10.1029/2025GC012881, Wiley Online Library on [07/11/2026]. See the Terms and Conditions (https://onlinelibrary.wiley.com/terms-and-conditions) on Wiley Online Library for rules of use; OA articles are governed by the applicable Creative Commons License

Haldan, M., Meijers, M., Langereis, C., Larsen, B., & Heyer, H. (2014). New palaeomagnetic results from the Oslo Graben, a Permian Superchron lava province. *Geophysical Journal International*, *199*(3), 1554–1571. https://doi.org/10.1093/gji/ggu351

Halls, H. C., Lovette, A., Hamilton, M., & Söderlund, U. (2015). A paleomagnetic and U–Pb geochronology study of the western end of the Grenville dyke swarm: Rapid changes in paleomagnetic field direction at ca. 585 Ma related to polarity reversals? *Precambrian Research*, *257*, 137–166. https://doi.org/10.1016/j.precamres.2014.11.029

Harrison, T. M., Duncan, I., & Mcdougall, I. (1985). Diffusion of 40Ar in biotite: Temperature, pressure and compositional effects. *Geochimica et Cosmochimica Acta*, *49*(11), 2461–2468. https://doi.org/10.1016/0016-7037(85)90246-7

Hospers, J. (1954). Rock magnetism and polar wandering. *The Journal of Geology*, *63*(1), 59–74. https://doi.org/10.1086/626226

Huang, W., Tarduno, J. A., Zhou, T., Ibañez-Mejia, M., Dal Olmo-Barbosa, L., Koester, E., et al. (2024). Near-collapse of the geomagnetic field may have contributed to atmospheric oxygenation and animal radiation in the Ediacaran Period. *Communications Earth and Environment*, *5*(1), 207. https://doi.org/10.1038/s43247-024-01360-4

Iosifidi, A., Khramov, A., & Bachtadse, V. (2005). Multicomponent magnetization of Vendian sedimentary rocks in Podolia, Ukraine. *Russian Journal of Earth Sciences*, *7*(1), 1–14. https://doi.org/10.2205/2004es000166

Jensen, H. G. (2017). *A study of highly oxidized, high-grade metamorphic sedimentary rocks-A geochemical and petrophysical study of rocks from the Modum Complex, South Norway (Thesis)*. NTNU.

Khramov, A. N. (1987). *Paleomagnetology*. Springer.

Kirschvink, J. (1980). The least-squares line and plane and the analysis of palaeomagnetic data. *Geophysical Journal International*, *62*(3), 699–718. https://doi.org/10.1111/j.1365-246X.1980.tb02601.x

Kirschvink, J. (1992). Late Proterozoic low-latitude global glaciation: The snowball Earth. In *The Proterozoic biosphere: A multidisciplinary Study*. Cambridge University Press.

Levashova, N. M., Bazhenov, M. L., Meert, J. G., Danukalov, K. N., Golovanova, I. V., Kuznetsov, N. B., & Fedorova, N. M. (2015). Paleomagnetism of upper Ediacaran clastics from the South Urals: Implications to paleogeography of Baltica and the opening of the Iapetus Ocean. *Gondwana Research*, *28*(1), 191–208. https://doi.org/10.1016/j.gr.2014.04.012

Levashova, N. M., Bazhenov, M. L., Meert, J. G., Kuznetsov, N. B., Golovanova, I. V., Danukalov, K. N., & Fedorova, N. M. (2013). Paleogeography of Baltica in the Ediacaran: Paleomagnetic and geochronological data from the clastic Zigan Formation, South Urals. *Precambrian Research*, *236*, 16–30. https://doi.org/10.1016/j.precamres.2013.06.006

Liu, Y.-S., Mitchell, R. N., Bleeker, W., Peng, P., Salminen, J., & Evans, D. A. (2024). Conformably variable geocentric axial dipole at ca. 2.1 Ga: Paleomagnetic dispersion of the Indin dyke swarm, Slave craton. *Journal of Geophysical Research: Solid Earth*, *129*(11), e2024JB029046. https://doi.org/10.1029/2024JB029046

Llanos, M. P. I., Tait, J. A., Popov, V., & Abalmassova, A. (2005). Palaeomagnetic data from Ediacaran (Vendian) sediments of the Arkhangelsk region, NW Russia: An alternative apparent polar wander path of Baltica for the Late Proterozoic–Early Palaeozoic. *Earth and Planetary Science Letters*, *240*(3–4), 732–747. https://doi.org/10.1016/j.epsl.2005.09.063

Lubnina, N. V., Pisarevsky, S. A., Puchkov, V. N., Kozlov, V. I., & Sergeeva, N. D. (2014). New paleomagnetic data from late Neoproterozoic sedimentary successions in Southern Urals, Russia: Implications for the late Neoproterozoic paleogeography of the Iapetan realm. *International Journal of Earth Sciences*, *103*(5), 1317–1334. https://doi.org/10.1007/s00531-014-1013-x

Maxbauer, D. P., Feinberg, J. M., & Fox, D. L. (2016). MAX UnMix: A web application for unmixing magnetic coercivity distributions. *Computers and Geosciences*, *95*, 140–145. https://doi.org/10.1016/j.cageo.2016.07.009

McFadden, P., & McElhinny, M. (1988). The combined analysis of remagnetization circles and direct observations in palaeomagnetism. *Earth and Planetary Science Letters*, *87*(1–2), 161–172. https://doi.org/10.1016/0012-821X(88)90072-6

Meert, J. G. (2009). In GAD we trust. *Nature Geoscience*, *2*(10), 673–674. https://doi.org/10.1038/ngeo635

Meert, J. G. (2014). Ediacaran–Early Ordovician paleomagnetism of Baltica: A review. *Gondwana Research*, *25*(1), 159–169. https://doi.org/10.1016/j.gr.2013.02.003

Meert, J. G., Pivarunas, A. F., Evans, D. A., Pisarevsky, S. A., Pesonen, L. J., Li, Z.-X., et al. (2020). The magnificent seven: A proposal for modest revision of the quality index. *Tectonophysics*, *790*, 228549. https://doi.org/10.1016/j.tecto.2020.228549

Meert, J. G., & Torsvik, T. H. (2004). Paleomagnetic constraints on Neoproterozoic "Snowball Earth" continental reconstructions. In G. S. Jenkins, M. A. McMenamin, C. P. McKay, & L. Sohl (Eds.), *Geophysical monograph series* (pp. 5–11). American Geophysical Union. https://doi.org/10.1029/146GM02

Meert, J. G., Torsvik, T. H., Eide, E. A., & Dahlgren, S. (1998). Tectonic significance of the Fen Province, S. Norway: Constraints from geochronology and paleomagnetism. *The Journal of Geology*, *106*(5), 553–564. https://doi.org/10.1086/516041

Meert, J. G., Walderhaug, H. J., Torsvik, T. H., & Hendriks, B. W. (2007). Age and paleomagnetic signature of the Alnø carbonatite complex (NE Sweden): Additional controversy for the Neoproterozoic paleoposition of Baltica. *Precambrian Research*, *154*(3–4), 159–174. https://doi.org/10.1016/j.precamres.2006.12.008

Neumann, E.-R., Olsen, K., Baldridge, W., & Sundvoll, B. (1992). The Oslo rift: A review. *Tectonophysics*, *208*(1–3), 1–18. https://doi.org/10.1016/0040-1951(92)90333-2

Phillips, B. R., Bunge, H.-P., & Schaber, K. (2009). True polar wander in mantle convection models with multiple, mobile continents. *Gondwana Research*, *15*(3–4), 288–296. https://doi.org/10.1016/j.gr.2008.11.007

Piper, J. (1981). Magnetic properties of the Alnøn complex. *Geologiska Foreningen i Stockholm Forhandlingar*, *103*(1), 9–15. https://doi.org/10.1080/11035898109455197

Piper, J. (1988). Palaeomagnetism of (late Vendian-earliest Cambrian) minor alkaline intrusions, Fen Complex, southeast Norway. *Earth and Planetary Science Letters*, *90*(4), 422–430. https://doi.org/10.1016/0012-821X(88)90140-9

Poorter, R. (1972). Preliminary palaeomagnetic results from the Fen carbonatite complex, S. Norway. *Earth and Planetary Science Letters*, *17*(1), 194–198. https://doi.org/10.1016/0012-821X(72)90276-2

Popov, V., Iosifidi, A., Khramov, A., Tait, J., & Bachtadse, V. (2002). Paleomagnetism of Upper Vendian sediments from the Winter Coast, White Sea region, Russia: Implications for the paleogeography of Baltica during Neoproterozoic times. *Journal of Geophysical Research*, *107*(B11), EPM–10. https://doi.org/10.1029/2001JB001607

Popov, V., Khramov, A., & Bachtadze, V. (2005). Paleomagnetism, magnetic stratigraphy and petromagnetism of the Upper Vendian sedimentary rocks in the sections of the Zolotitsa River and in the Verkhotina Hole, Winter Coast of the White Sea, Russia. *Russian Journal of Earth Sciences*, *7*, 1–29.

Pu, J. P., Bowring, S. A., Ramezani, J., Myrow, P., Raub, T. D., Landing, E., et al. (2016). Dodging snowballs: Geochronology of the Gaskiers glaciation and the first appearance of the Ediacaran biota. *Geology*, *44*(11), 955–958. https://doi.org/10.1130/G38284.1

Puchkov, V. (2012). On the age of the Asha series, South Urals. In *Geology, mineral resources, and geoecological problems of Bashkortostan, Ural, and adjacent areas: Proceedings of the IX interregional science-and-practice conference* (pp. 47–51). Ufa.

15252027, 2026, 5, Downloaded from https://agupubs.onlinelibrary.wiley.com/doi/10.1029/2025GC012881, Wiley Online Library on [07/11/2026]. See the Terms and Conditions (https://onlinelibrary.wiley.com/terms-and-conditions) on Wiley Online Library for rules of use; OA articles are governed by the applicable Creative Commons License

Robert, B., Corfu, F., Domeier, M., & Blein, O. (2023). Evidence for large disturbances of the Ediacaran geomagnetic field from West Africa. *Precambrian Research*, *394*, 107095. https://doi.org/10.1016/j.precamres.2023.107095

Robinson, P., Langenhorst, F., McEnroe, S., Fabian, K., & Ballaran, T. B. (2014). Ferroan geikielite and coupled spinel-rutile exsolution from titanohematite: Interface characterization and magnetic properties. *American Mineralogist*, *99*(8–9), 1694–1712. https://doi.org/10.2138/am.2014.4711

Runcorn, S. K. (1962). *Continental drift* (Vol. 3). Elsevier.

Sæther, E. (1957). The alkaline rock province of the Fen area in Southern Norway. *Det Konglige Norske Vitensk. Selsk., Skr.*, *1*, 1–150.

Schmidt, P. (1993). Palaeomagnetic cleaning strategies. *Physics of the Earth and Planetary Interiors*, *76*(1–2), 169–178. https://doi.org/10.1016/0031-9201(93)90066-I

Schwarz, E. J., & Buchan, K. L. (1989). Identifying types of remanent magnetization in igneous contact zones. *Physics of the Earth and Planetary Interiors*, *58*(2–3), 155–162. https://doi.org/10.1016/0031-9201(89)90051-4

Środoń, J., Gerdes, A., Kramers, J., & Bojanowski, M. J. (2022). Age constraints of the Sturtian glaciation on western Baltica based on U-Pb and Ar-Ar dating of the Lapichi Svita. *Precambrian Research*, *371*, 106595. https://doi.org/10.1016/j.precamres.2022.106595

Sundvoll, B., & Larsen, B. (1990). Rb-Sr isotope systematics in the magmatic rocks of the Oslo rift. *NGU Bulletin*, *418*, 27–46.

Sundvoll, B., & Larsen, B. (1994). Architecture and early evolution of the Oslo Rift. *Tectonophysics*, *240*(1–4), 173–189. https://doi.org/10.1016/0040-1951(94)90271-2

Tarduno, J. A., Zhou, T., Huang, W., & Jodder, J. (2025). Earth's magnetic field and its relationship to the origin of life, evolution and planetary habitability. *National Science Review*, *12*(5). https://doi.org/10.1093/nsr/nwaf082

Tauxe, L. (2010). *Essentials of paleomagnetism*. University of California Press.

Tauxe, L., Shaar, R., Jonestrask, L., Swanson-Hysell, N. L., Minnett, R., Koppers, A. A. P., et al. (2016). PmagPy: Software package for paleomagnetic data analysis and a bridge to the Magnetics Information Consortium (MagIC) Database. *Geochemistry, Geophysics, Geosystems*, *17*(6), 2450–2463. https://doi.org/10.1002/2016GC006307

Thallner, D., Biggin, A. J., & Halls, H. C. (2021). An extended period of extremely weak geomagnetic field suggested by palaeointensities from the Ediacaran Grenville dykes (SE Canada). *Earth and Planetary Science Letters*, *568*, 117025. https://doi.org/10.1016/j.epsl.2021.117025

Tonti-Filippini, J. A. D., & Gilder, S. A. (2023). Vector unmixing of multicomponent palaeomagnetic data. *Geophysical Journal International*, *233*(3), 1632–1654. https://doi.org/10.1093/gji/ggac505

Tonti-Filippini, J. A. D., Antonio, P. Y. J., Dahlgren, S., de Boer, R., Gallo, L., Silkoset, P., et al. (2026). Ediacara obscura: Unveiling hidden magnetisations in the Fen complex, southern Norway [Dataset]. *MagIC database*. https://doi.org/10.7288/V4/MAGIC/20274

Torsvik, T. H., & Cocks, L. R. M. (2017). *Earth history and palaeogeography*. Cambridge University Press.

Torsvik, T. H., Eide, E. A., Meert, J. G., Smethurst, M. A., & Walderhaug, H. J. (1998). The Oslo Rift: New palaeomagnetic and 40Ar/39Ar age constraints. *Geophysical Journal International*, *135*(3), 1045–1059. https://doi.org/10.1046/j.1365-246X.1998.00687.x

Torsvik, T. H., Van der Voo, R., Preeden, U., Mac Niocaill, C., Steinberger, B., Doubrovine, P. V., et al. (2012). Phanerozoic polar wander, palaeogeography and dynamics. *Earth-Science Reviews*, *114*(3–4), 325–368. https://doi.org/10.1016/j.earscirev.2012.06.007

Tsai, V. C., & Stevenson, D. J. (2007). Theoretical constraints on true polar wander. *Journal of Geophysical Research*, *112*(B5). https://doi.org/10.1029/2005JB003923

Van Der Voo, R. (1990). The reliability of paleomagnetic data. *Tectonophysics*, *184*(1), 1–9. https://doi.org/10.1016/0040-1951(90)90116-P

Walderhaug, H. J., Torsvik, T. H., & Halvorsen, E. (2007). The Egersund dykes (SW Norway): A robust early Ediacaran (Vendian) palaeomagnetic pole from Baltica. *Geophysical Journal International*, *168*(3), 935–948. https://doi.org/10.1111/j.1365-246X.2006.03265.x

Xue, Y., Domeier, M., Silkoset, P., Gallo, L. C., Tonti-Filippini, J. A. D., & Walderhaug, H. (2026). Cryptic paleomagnetic complexity in the Ediacaran Egersund dikes. *Geochemistry, Geophysics, Geosystems*, *27*(5), e2025GC012730. https://doi.org/10.1029/2025GC012730

Zahirovic, S., Müller, R. D., Seton, M., & Flament, N. (2015). Tectonic speed limits from plate kinematic reconstructions. *Earth and Planetary Science Letters*, *418*, 40–52. https://doi.org/10.1016/j.epsl.2015.02.037

Zaitseva, T., Kuznetsov, A., Gorozhanin, V., Gorokhov, I., Ivanovskaya, T., & Konstantinova, G. (2019). The lower boundary of the Vendian in the Southern Urals as evidenced by the Rb–Sr age of glauconites of the Bakeevo Formation. *Stratigraphy and Geological Correlation*, *27*(5), 573–587. https://doi.org/10.1134/S0869593819050083

Zijderveld, J. (1967). A. C. Demagnetization of rocks: Analysis of results. In *Developments in solid Earth geophysics* (Vol. 3, pp. 254–286). Elsevier. https://doi.org/10.1016/b978-1-4832-2894-5.50049-5

References From the Supporting Information

Griffin, W. L., & Taylor, P. N. (1975). The Fen damkjernite: Petrology of a "central-complex kimberlite". *Physics and Chemistry of the Earth*, *9*, 163–177. https://doi.org/10.1016/0079-1946(75)90015-4

15252027, 2026, 5, Downloaded from https://agupubs.onlinelibrary.wiley.com/doi/10.1029/2025GC012881, Wiley Online Library on [07/11/2026]. See the Terms and Conditions (https://onlinelibrary.wiley.com/terms-and-conditions) on Wiley Online Library for rules of use; OA articles are governed by the applicable Creative Commons License